Chapter 19

General Circulation Modeling and the Tropics

Jagadish Shukla

General circulation models (GCMs) are used to simulate atmospheric climate. These models are three-dimensional and represent the atmosphere by layers in the vertical dimension, typically about 10, and by grid points or Fourier (spectral) waves in the horizontal dimension, with typical resolution of about five degrees of latitude and longitude. Atmospheric winds are obtained by solution of the fluid equations of motion with numerical approximations defined on the model grid. Likewise, the distributions of temperature, humidity, pressure, and rainfall are calculated by numerical approximations to the continuum equations and parameterizations of the subgrid-scale processes. GCMs are used for sensitivity studies of atmospheric circulation. Models can be integrated with and without a prescribed change (e.g., deforestation) to calculate responses to the prescribed change.

The main emphasis in this essay is the simulation of tropical climate and its interannual variability. However, since tropical and extratropical variability are closely related, it is difficult to isolate the tropics in a global GCM. Therefore, we present the modeling of global circulation with particular emphasis on the tropics.

The ability and limitations of the GCMs to simulate climate and its variability are discussed in terms of

a. mean climate;
b. space–time fluctuations within a season;
c. interannual variability of monthly, seasonal, and annual means; and
d. interannual variability of intraseasonal space–time fluctuations.

For a description of the simulation of the mean climate, we have summarized the results of Shukla et al. (1981a) and for interannual variability the results of Manabe and Hahn (1981), Charney and Shukla (1981), Lau (1981), Lau and Oort (1984), Malone et al. (1984) and Lau (1985). For additional discussion of simulation of tropical mean and transient circulations, the reader is referred to pioneering works of Manabe and his colleagues (Manabe and Smagorinsky, 1967; Manabe et al., 1970; Manabe et al., 1974; Hayashi, 1974; Hayashi and Golder, 1980).

MEAN CLIMATE

The time-averaged circulation or the *mean climate* of the atmosphere is determined by a balance between the radiative forcing (shortwave and longwave radiation), the stationary forcing at the earth's surface (resulting from mountains and land, ocean, and ice distribution), and the horizontal and vertical fluxes of heat, momentum, and moisture. For a realistic simulation of the mean climate, it is therefore necessary to calculate each of these components accurately. Calculation of radiative fluxes requires vertical profiles of temperature, moisture, O_3, CO_2, other trace gases and aerosols, and a treatment of cloud–radiation interaction for variable clouds. To accurately calculate the stationary forcing at the earth's surface, it is necessary to model correctly the thermal and mechanical effects of mountains and the heat and moisture fluxes across land–air, sea–air, snow–air, and ice–air interfaces. And finally, an accurate calculation of the dynamical fluxes requires the simulation of the correct amplitudes and phases of stationary and transient eddies, their growth and decay, and their interactions among themselves and with the mean circulation.

One of the primary objectives of general circulation modeling studies has been to simulate the mean climate realistically by incorporating these complex processes in a single model. All the physical-dynamical processes discussed above have not been treated with a uniform degree of sophistication. Some processes have been treated in detail, whereas other processes are highly simplified. The large number of parameters and processes has made it difficult to conduct extensive integrations to determine the appropriate levels of complexity for treatment of physical processes. Therefore, it is very difficult to compare the models with each other; rather, each model is compared individually with observations.

The discussions in this chapter are confined to comparisons with observations, and no attempt is made to describe the model sensitivity to external forcings, parameterizations of physical processes, and chemical composition.

We present here a summary of simulation results from the GLAS (Goddard Laboratory for Atmospheric Sciences) climate model, which has been extensively described in Shukla et al. (1981a).

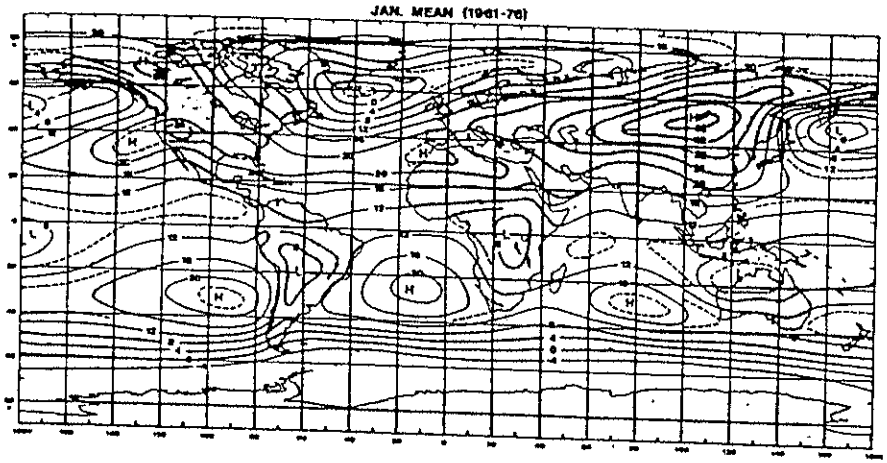

(a)

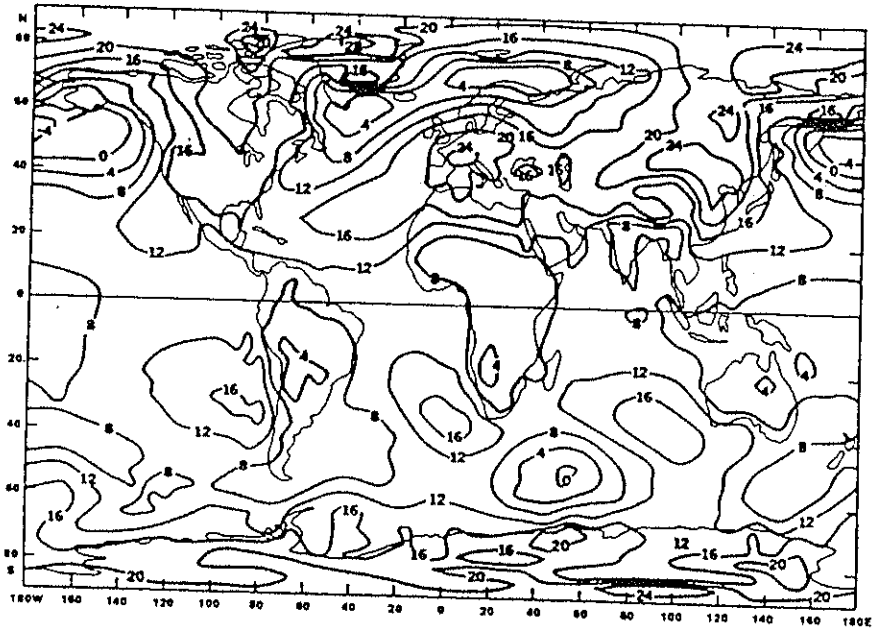

(b)

FIGURE 1. Mean sea level pressure (−1000 mb): (*a*) observed January (Godbole and Shukla, 1981); (*b*) GCM February; (*c*) observed July (Godbole and Shukla, 1981); (*d*) GCM July.

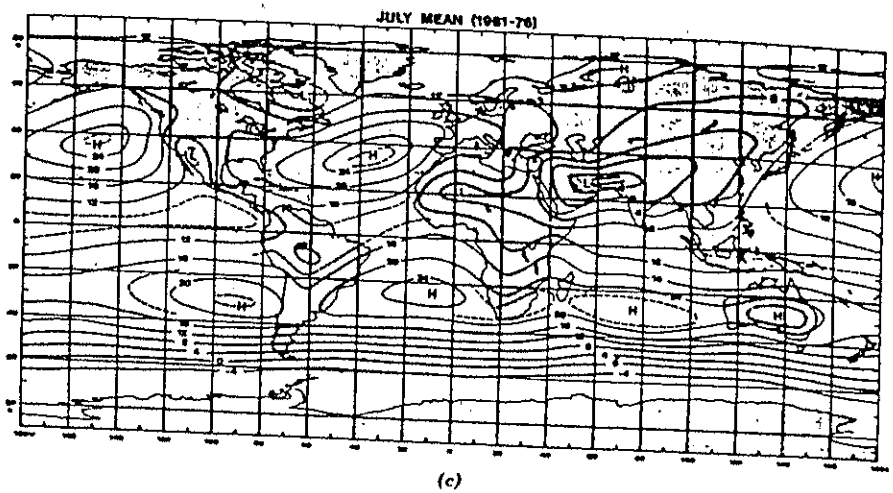

(c)

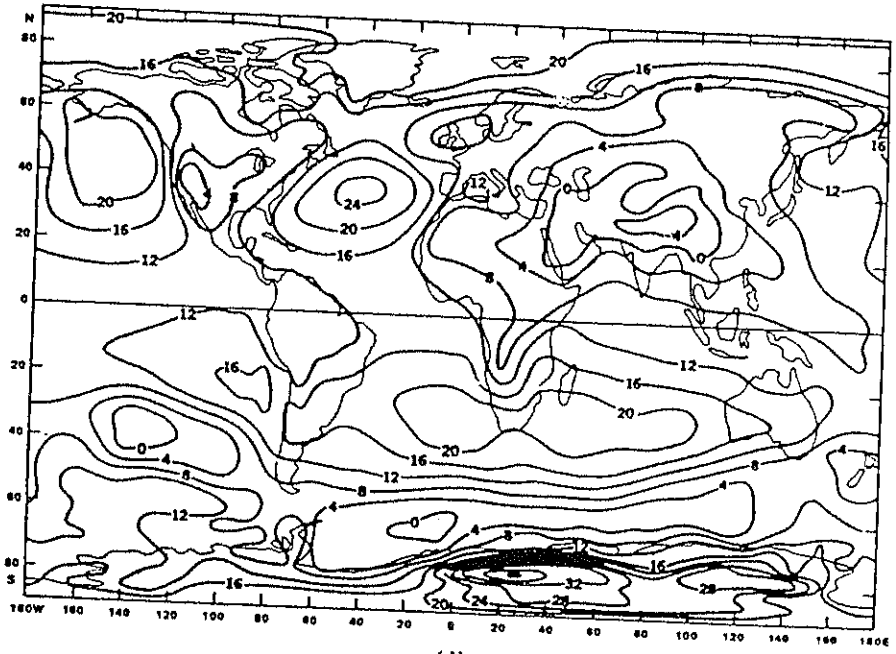

(d)

FIGURE 1. (*continued*)

Sea Level Pressure

Figures 1*a* and 1*c* show the observed 16-y mean sea level pressure for January and July reproduced from Godbole and Shukla (1981), and Figures 1*b* and 1*d* show the model's simulated mean sea level pressure for a single February and July, respectively. For February, the simulation of the prom-

inent Northern Hemispheric circulation features, such as the Aleutian and Icelandic lows, is fairly realistic, but the discrepancy in the structure and intensity of the Siberian high is too large to be accounted for by interannual variability or by differences between January and February. The most serious deficiency of the simulated field is in the Southern Hemisphere, south of 60°S, where the simulated field shows a large eddy structure whereas the observed field is zonally uniform. For July, the high-pressure cell over the North Atlantic and the monsoon low are well simulated, but the orientation of the North Pacific high is not as observed. The subtropical high-pressure cells in the Southern Hemisphere are well simulated over the Indian Ocean, Atlantic Ocean, and eastern Pacific but not over Australia. For both summer and winter, the models show a common deficiency of distinct nonzonal isobar configurations in the Southern Hemispheric mid-to-high latitudes.

Geopotential Height

Figure 2 shows the observed and simulated geopotential height field at 200 mb. For February, the simulated trough over northeast United States and eastern Canada, the ridge over the eastern Atlantic, the jet stream over Japan, and the anticyclonic circulation over the tropics are quite realistic. However, the ridge over the west coast of the United States is displaced to the east, and the Southern Hemisphere midlatitudes show more eddy structure than is observed. For July, there are several deficiencies in the simulated field. Large-amplitude short waves are seen over North America and adjacent Pacific Ocean, and the geopotential heights in the tropical belt are higher by about 200 geopotential meter (gpm) than is observed.

The surface circulation during July and the upper-level circulation during February are, in general, better simulated than the surface circulation during February and the upper-level circulation during July.

Zonal Wind and Temperature

Figure 3 shows the observed and simulated zonal wind and zonally averaged temperature. For February, the locations of the strongest zonal wind maxima in both hemispheres are well simulated. The most conspicuous deficiency is the absence of the closed maximum near 200 mb that is seen in the observed zonal winds. This deficiency is related to the very low model temperatures in the upper troposphere of the polar regions. The model-simulated tropical atmosphere is considerably warmer than the observed atmosphere. Cooling near the poles and large zonal winds near the upper boundary have been one of the common deficiencies of GCMs, and their precise cause is yet to be determined.

Stationary Wave Variance

Figure 4 shows the observed and simulated variances around a latitude circle of the winter and summer mean stationary geopotential height summed over

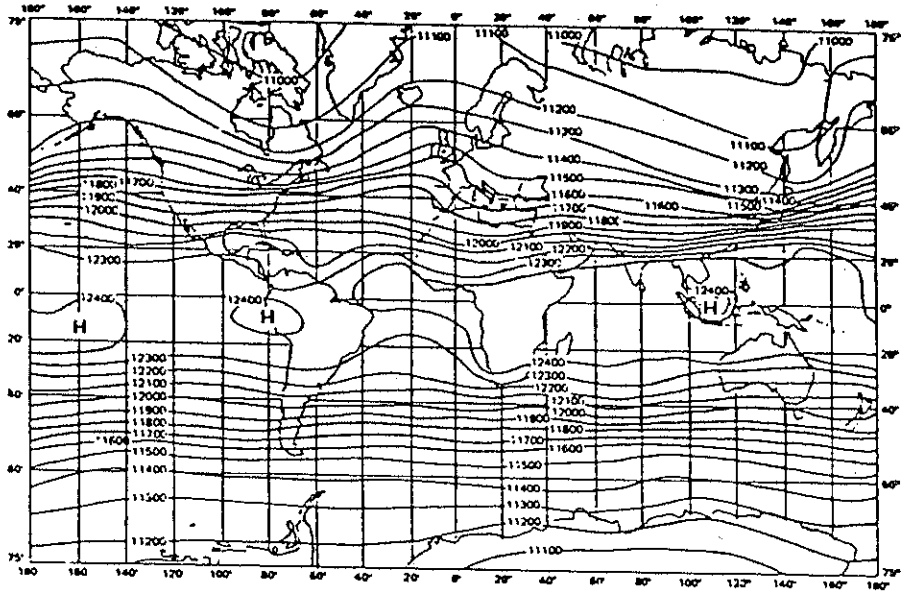

(a)

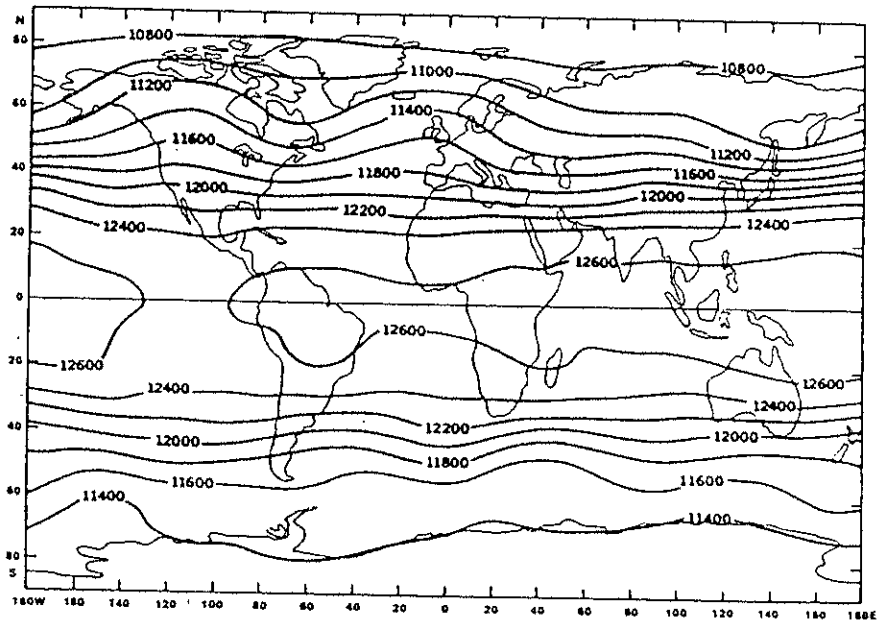

(b)

FIGURE 2. Mean geopotential height (m) at 200 mb: (a) observed December, January, and February; (b) GCM February; (c) observed June, July, and August, (d) GCM July.

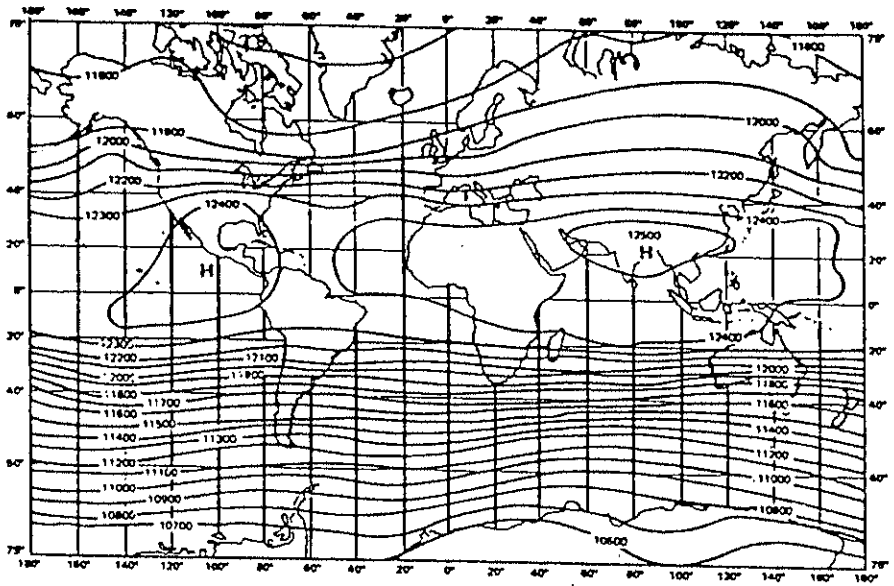

(c)

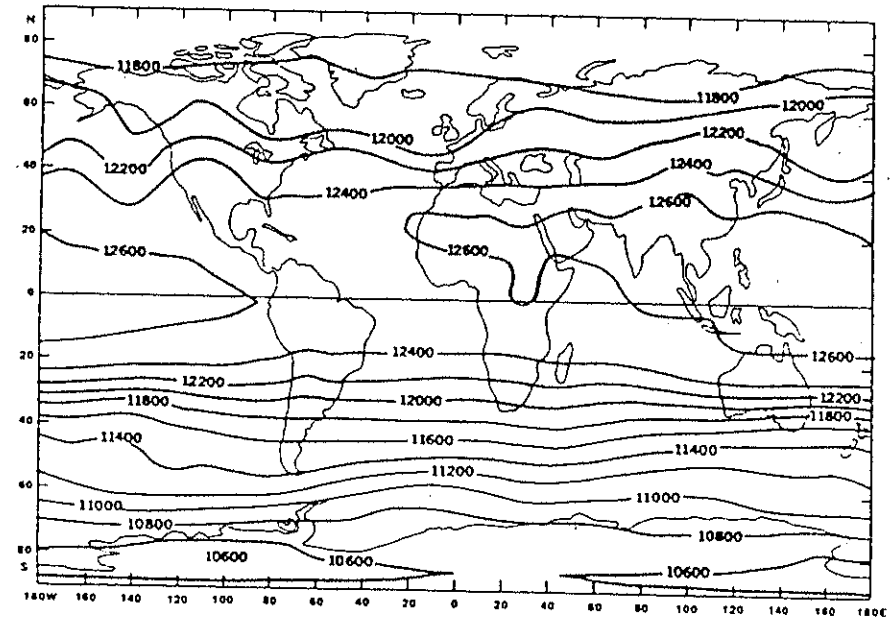

(d)

FIGURE 2. (*continued*)

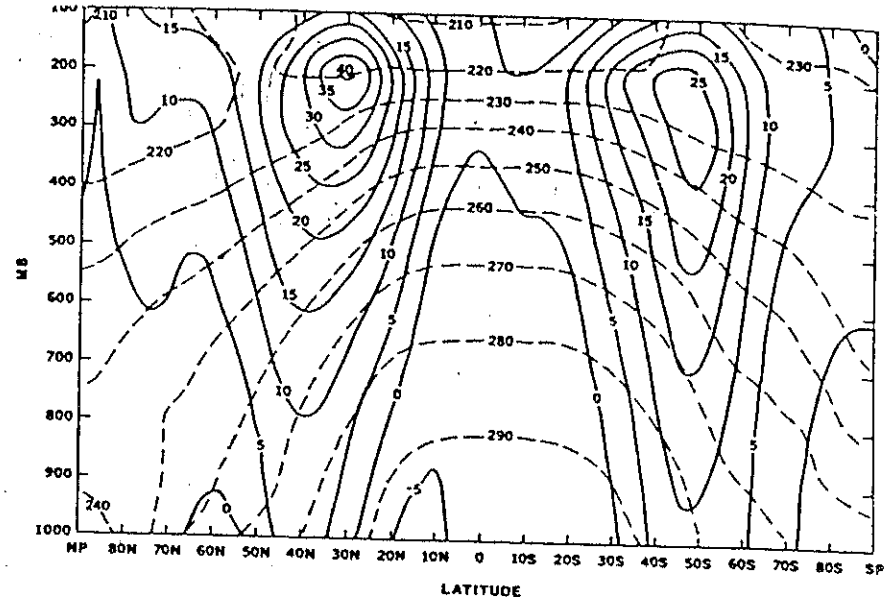

(a)

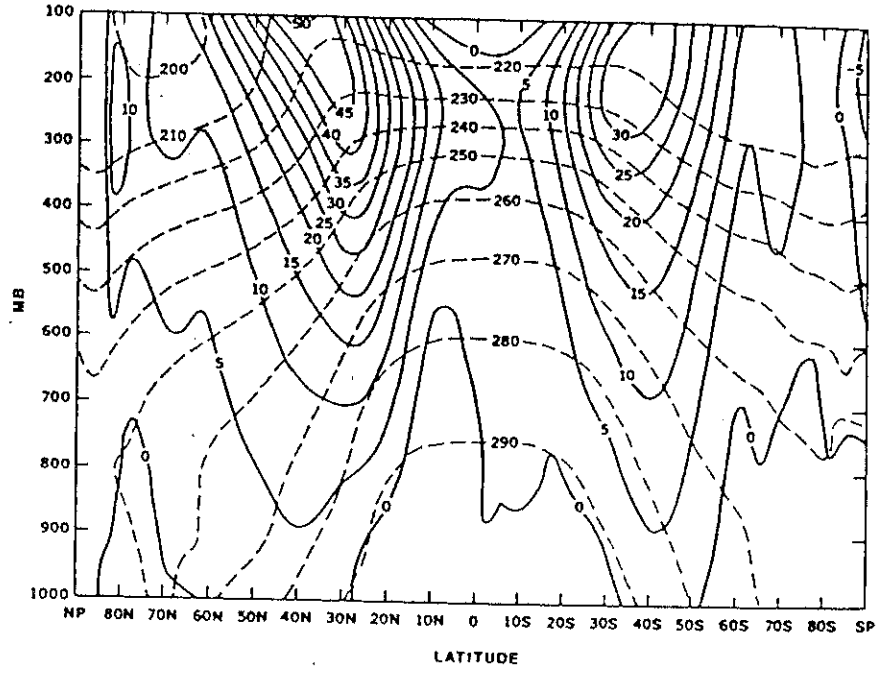

(b)

FIGURE 3. Zonally averaged zonal wind (m s^{-1} solid lines) and temperature (K, dashed lines): (*a*) observed February, 1979; (*b*) GCM February; (*c*) observed July 1979; (*d*) GCM July.

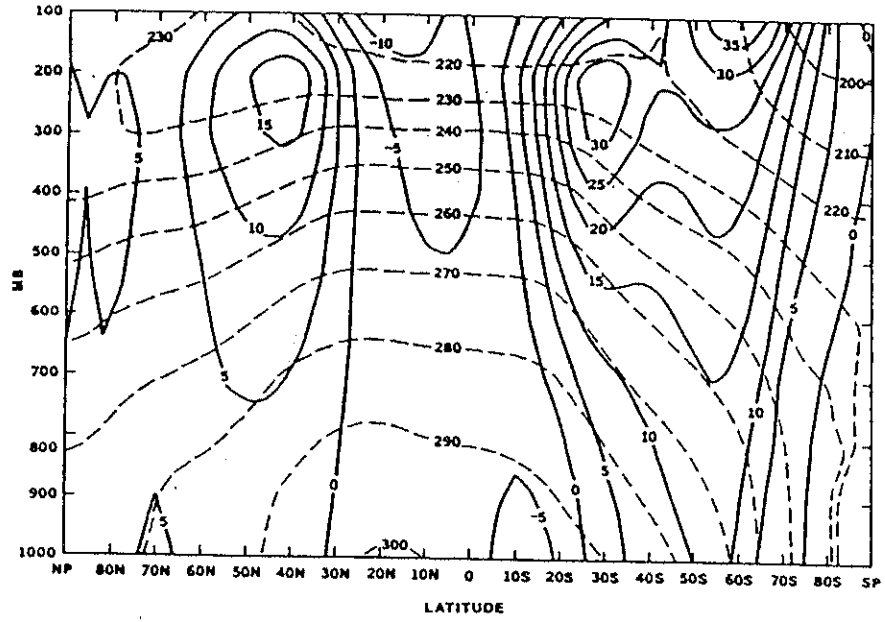

(c)

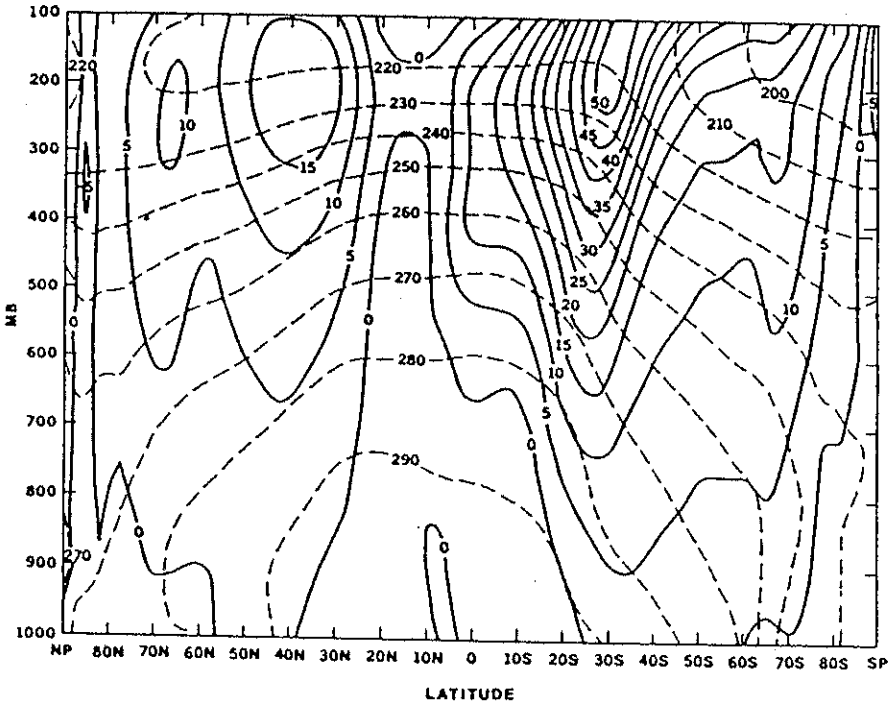

(d)

FIGURE 3. (*continued*)

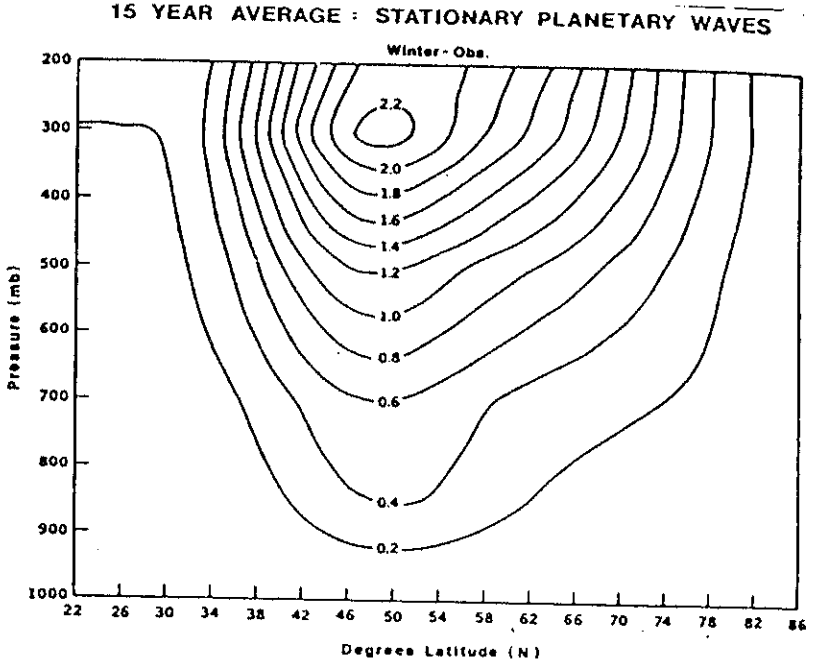

(a)

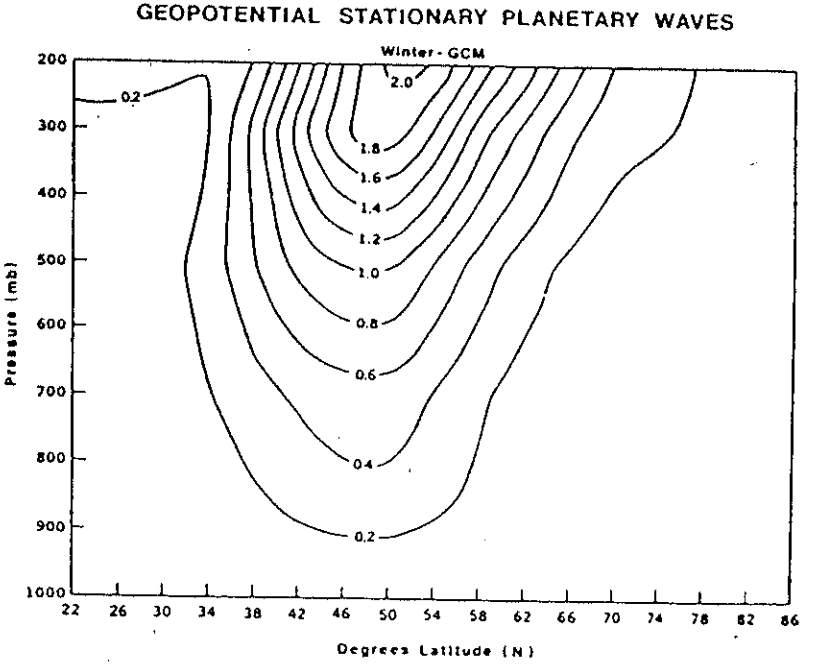

(b)

FIGURE 4. Stationary planetary wave variance of the geopotential height in the Northern Hemisphere: (*a*) observed winter (units of 10^4 m^2); (*b*) GCM winter (units of 10^4 m^2); (*c*) observed summer (units of 10^3 m^2), (*d*) GCM summer (units of 10^3 m^2).

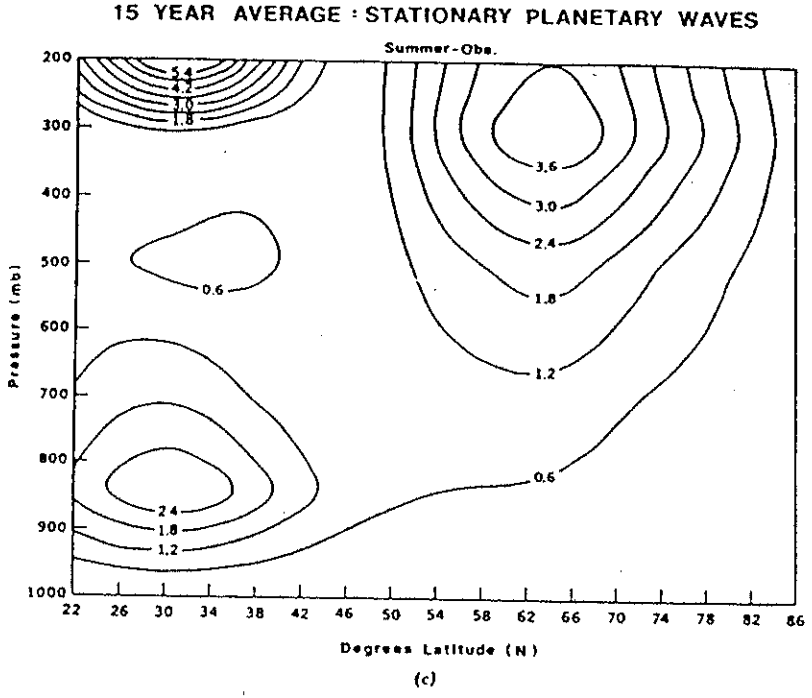

FIGURE 4. (*continued*)

the planetary waves (wave number 1–4). The latitudinal and height distributions of the simulated variance are in good agreement with the observations for both seasons. The observed decrease of variance above 300 mb is not satisfactorily simulated. This discrepancy is probably related to the low polar temperatures and strong zonal winds at the upper levels.

Surface Winds and ITCZ

Figures 5 and 6 show the observed and simulated surface winds reported in the modeling study of Halem et al. (1979). The corresponding maps from Shukla et al. (1981a) are quite similar to these. The observed fields are from Mintz and Dean (1952). The agreement between the observed and the simulated intertropical convergence zone (ITCZ) is very good, especially with regard to its longitudinal variation. The structure and locations of anticyclonic centers are also well simulated. The seasonal reversal from northeasterly winds during winter to southwesterly winds during summer over the north Indian Ocean is correctly simulated by the model. The main discrepancy in the latitudinal location of ITCZ occurs during winter over the eastern part of the Pacific and over the Indian Ocean.

Rainfall

Figures 7 and 8 show the observed (from Jaeger, 1976) and simulated monthly mean rainfall for winter and summer, respectively. Given the large variability of rainfall and the uncertainty in the observations, the agreement between the simulated and the observed rainfall patterns is very good. Areas of very large and very small rainfall are well reproduced. The most obvious discrepancies are the excessive February precipitation over the Tibetan plateau and the overprediction of July rainfall over eastern North America. Partition of the total precipitation between large-scale and convective (cumulus) precipitation (not shown) indicates that in both seasons cumulus precipitation dominates in the tropics but large-scale precipitation dominates in higher latitudes.

Upper-Level Flow

The simulation of the 200-mb flow (not shown) by Shukla et al. (1981a) is in good agreement with the observations. For February, the locations and the intensities of the jet streams in both hemispheres are well simulated, although the simulated jet stream speeds were stronger than those observed for 1979, to which they are compared in Shukla et al.

Manabe et al. (1979) have presented simulation results from spectral models with 15, 21, and 30 wave numbers. They found that the increase in spectral resolution improved the simulation of tropical rain belts and subtropical dry zones. An example of one of the better simulations of the upper-

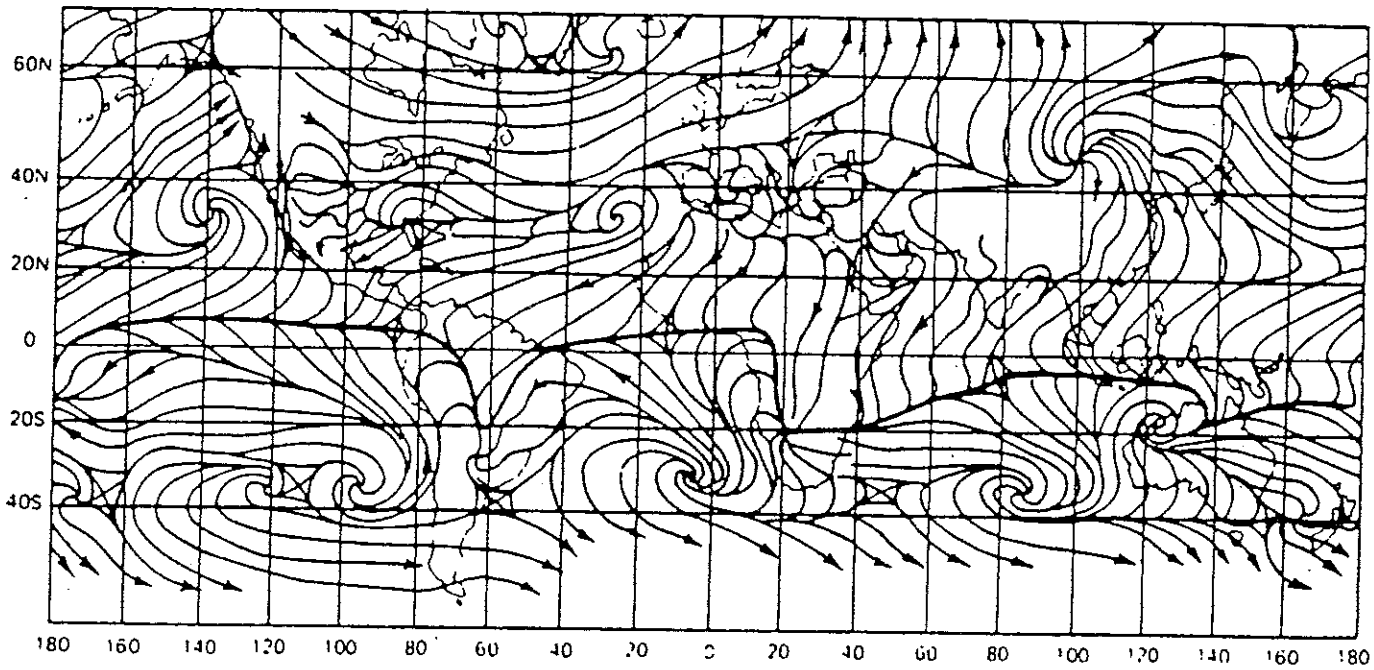

(a)

FIGURE 5. Streamlines at earth surface: (*a*) observed January (Mintz and Dean, 1952); (*b*) GCM February. [From Halem et al. (1979) with permission of the World Meteorological Organization.]

421

422

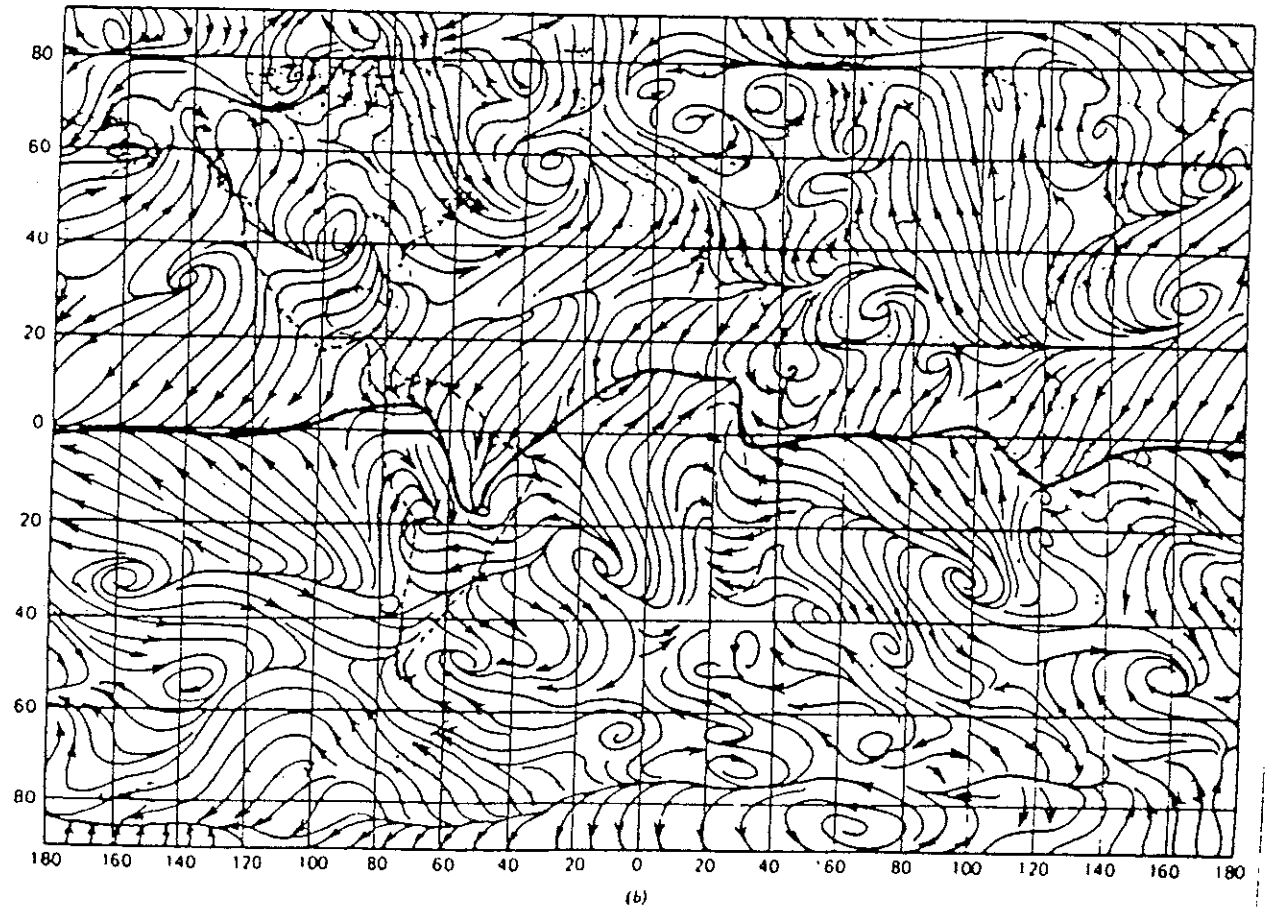

(b)

FIGURE 5 (continued)

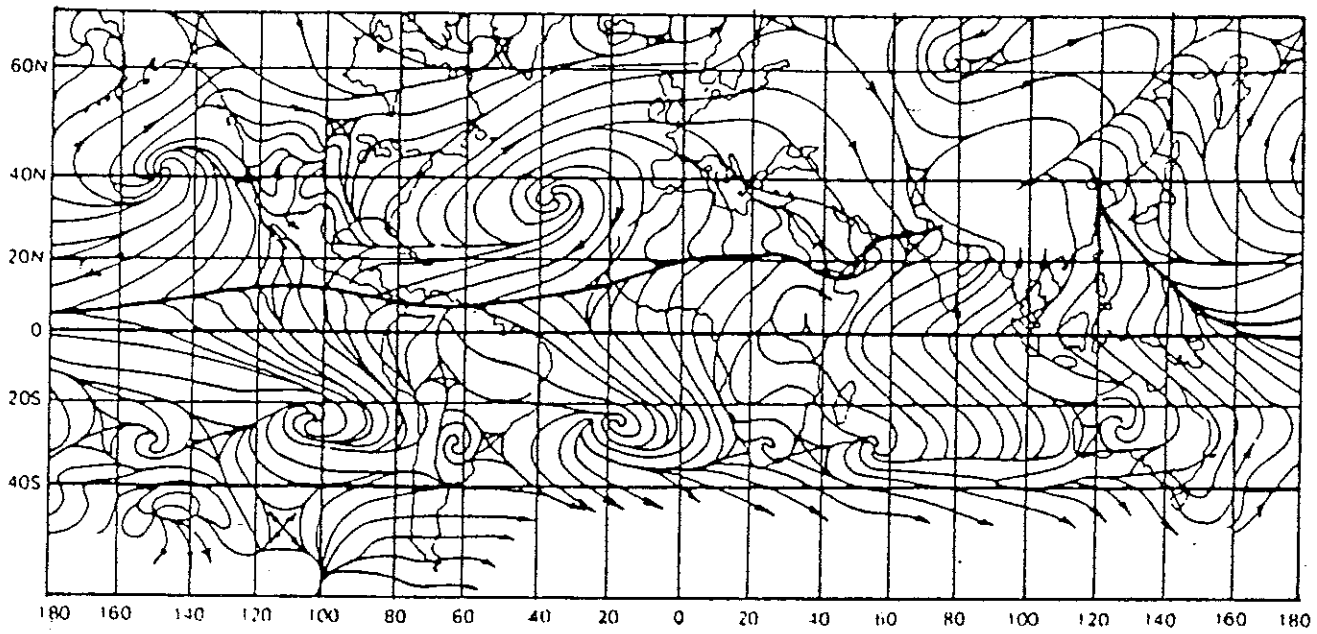

(a)

FIGURE 6. Streamlines at earth surface: (*a*) observed July (Mintz and Dean, 1952); (*b*) GCM July. [From Halem et al. (1979) with permission of the World Meteorological Organization.]

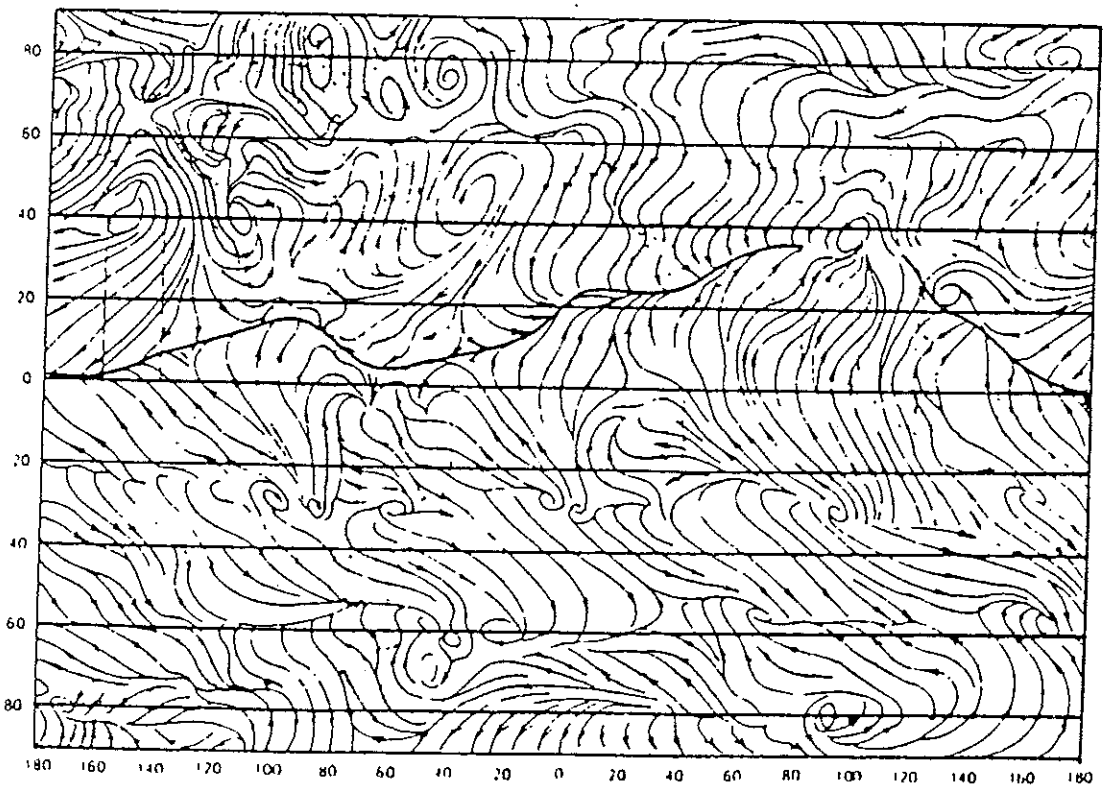

(b)

FIGURE 6. (*continued*)

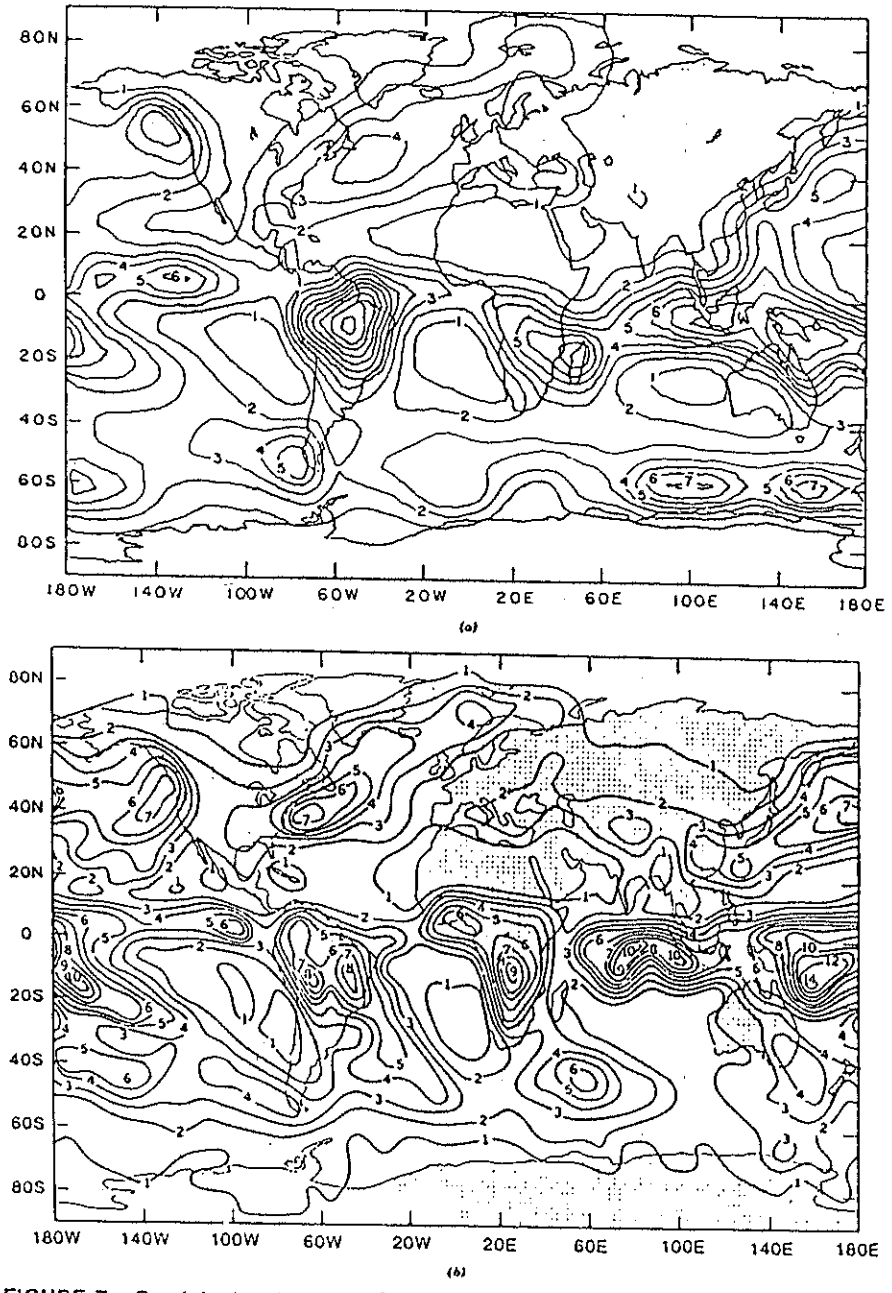

FIGURE 7. Precipitation (mm day^{-1}): (*a*) observed February (Jaeger, 1976); (*b*) GCM February.

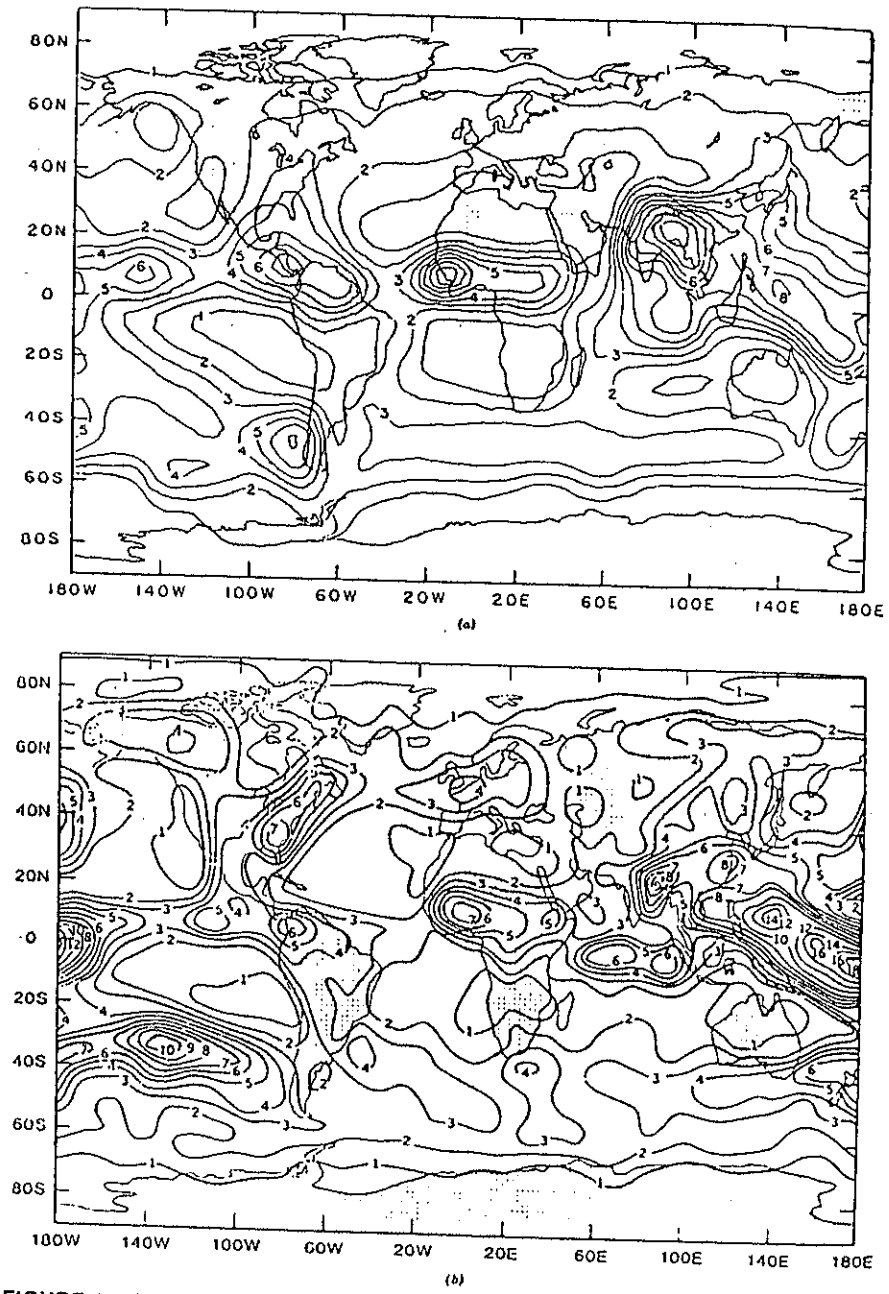

FIGURE 8. Precipitation (mm day^{-1}): (*a*) observed July (Jaeger, 1976); (*b*) GCM July.

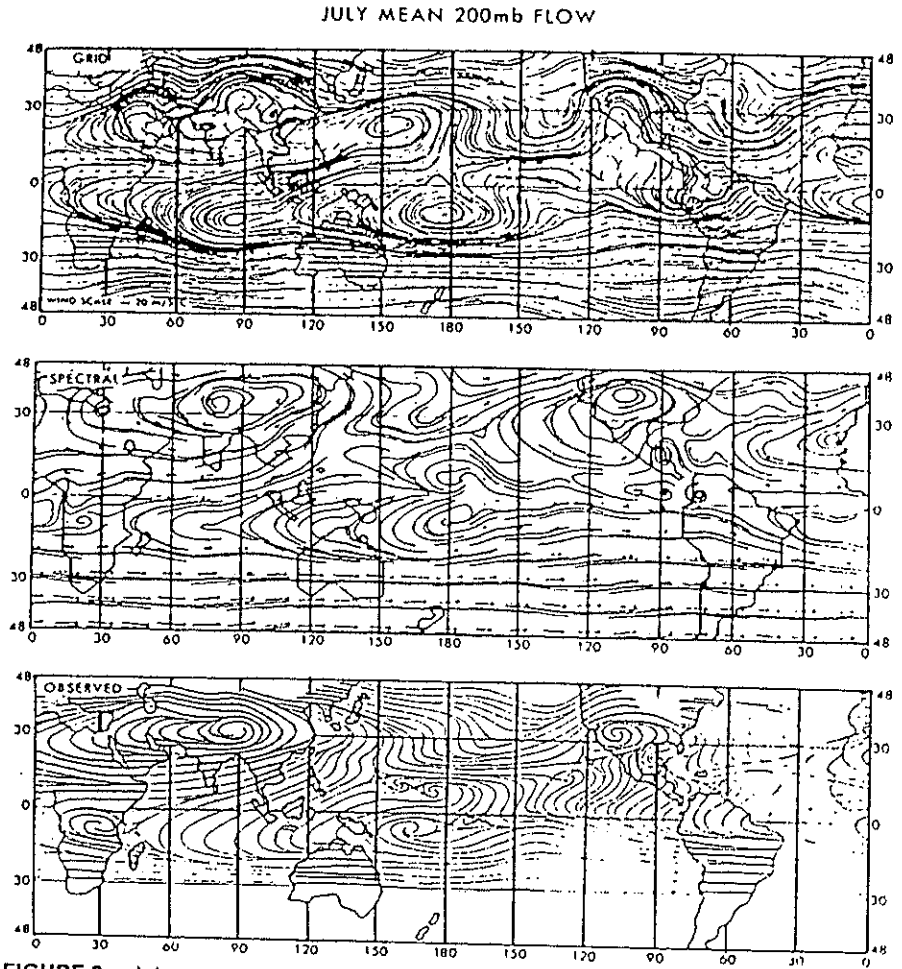

FIGURE 9. July mean streamlines: (*top*) computed at 190 mb (grid model, Manabe et al., 1974; (*middle*) computed at 205 mb [spectral model, from Manabe et al. (1979)]; (*bottom*) observed at 200 mb (Sadler, 1975).

level flow with a 30-wave-number spectral model is shown in Fig. 9, reproduced from Hayashi (1980). The large-scale features of the Tibetan and Mexican highs, the mid-Pacific and mid-Atlantic troughs, and the easterly jet off southern Asia are better simulated in the spectral model than in the grid model.

SPACE–TIME FLUCTUATIONS WITHIN A SEASON

For GCMs to be useful for sensitivity and predictability studies, they must simulate accurately not only the time-averaged circulation but also the transient circulation. We present here the simulation of low-frequency planetary wave variance and the local bandpass variance from the GLAS climate model and the Geophysical Fluid Dynamics Laboratory of NOAA (GFDL) grid point model.

Low-Frequency Planetary Wave (LFPW) Variance

The LFPWs consist of wave numbers 1–4 with periods of 7.5–90 days. Figure 10 shows the observed and simulated latitude–height structure of the LFPWs. There is general agreement in the overall structure for both winter and summer seasons. The discrepancy near the upper level is the same as discussed for Figure 4; in addition, the model variances are somewhat too small.

Bandpass Variance

Figure 11 shows the observed and simulated local bandpass filtered variance of the 500-mb geopotential height in the Northern Hemisphere for the winter season. The bandpass variance is defined as the spatially local root-mean square (rms) deviation in time for fluctuations of 2.5–6 days. The bandpass variance is related to the frequency, intensity, growth, and decay of cyclonic storms and indicates the location of "storm tracks" (Blackmon et al., 1977). The observed and simulated bandpass rms for winter are in excellent agreement in both the location and the strength of the major areas of cyclonic activity in the north central Pacific and western Atlantic. For summer (not shown) the Atlantic maximum has been realistically simulated, both with respect to position and to magnitude, but the simulated Pacific maximum is too weak and is located too far to the west.

Blackmon and Lau (1980) have analyzed the variance and covariance of bandpass filtered and low-pass filtered data from simulations of a GFDL model earlier described by Manabe et al. (1974). They found good agreement between the observations and the model-simulated location and intensity of storm tracks, vertical structure of the disturbances, and transport of heat and potential vorticity by transient eddies. The total rms and the low-pass filtered rms of the 500-mb height were weaker in the model simulations than in the observations.

Malone et al. (1984) have presented the results of simulation of stationary and transient eddies using the spectral general circulation model (Pitcher et al., 1983). In general, simulation of stationary waves is more realistic in the Northern Hemisphere than in the Southern Hemisphere. The transient eddies are better simulated in the winter hemisphere; however, for geopotential height the total variance at 400 mb is too high and bandpass variance at 1000 mb is too low over the Northern Hemisphere for January simulation. The structure of the transient wave variability in the summer hemisphere also shows some discrepancies from the observations.

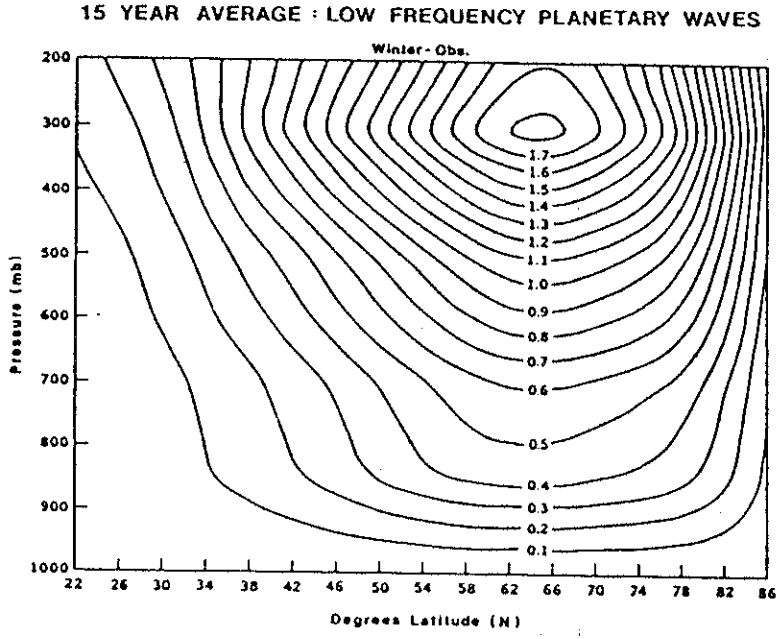

FIGURE 10. Geopotential height variance in low-frequency planetary waves in the Northern Hemisphere: (*a*) observed winter (in units of 10^4 m^2, contour interval is 0.1 × 10^4 m^2); (*b*) GCM winter (10^4 m^2, contour interval 0.1 × 10^4 m^2); (*c*) observed summer (10^3 m^2, contour interval 0.9 × 10^3 m^2); (*d*) GCM summer (10^3 m^2, contour interval 1.0 × 10^3 m^2).

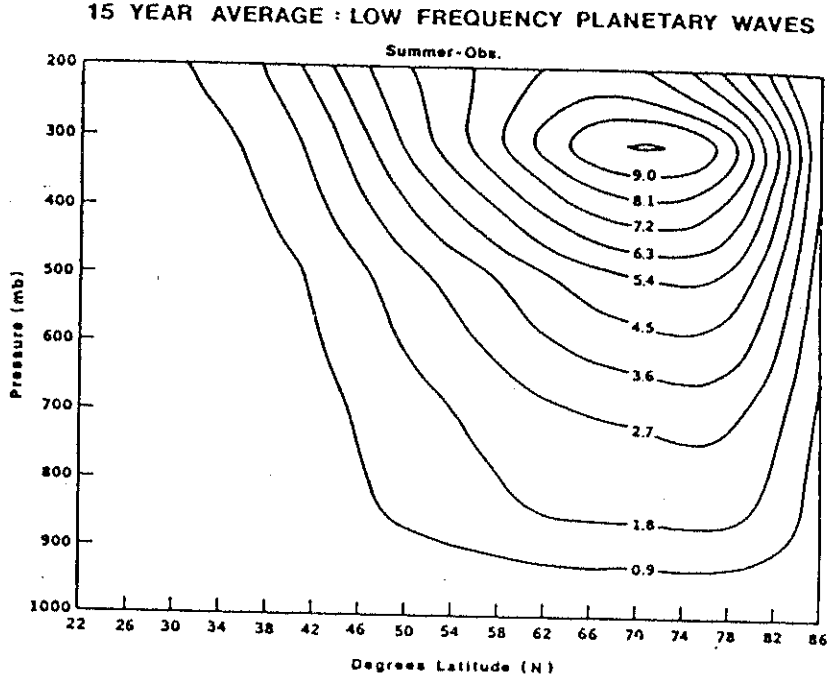

FIGURE 10. (*continued*)

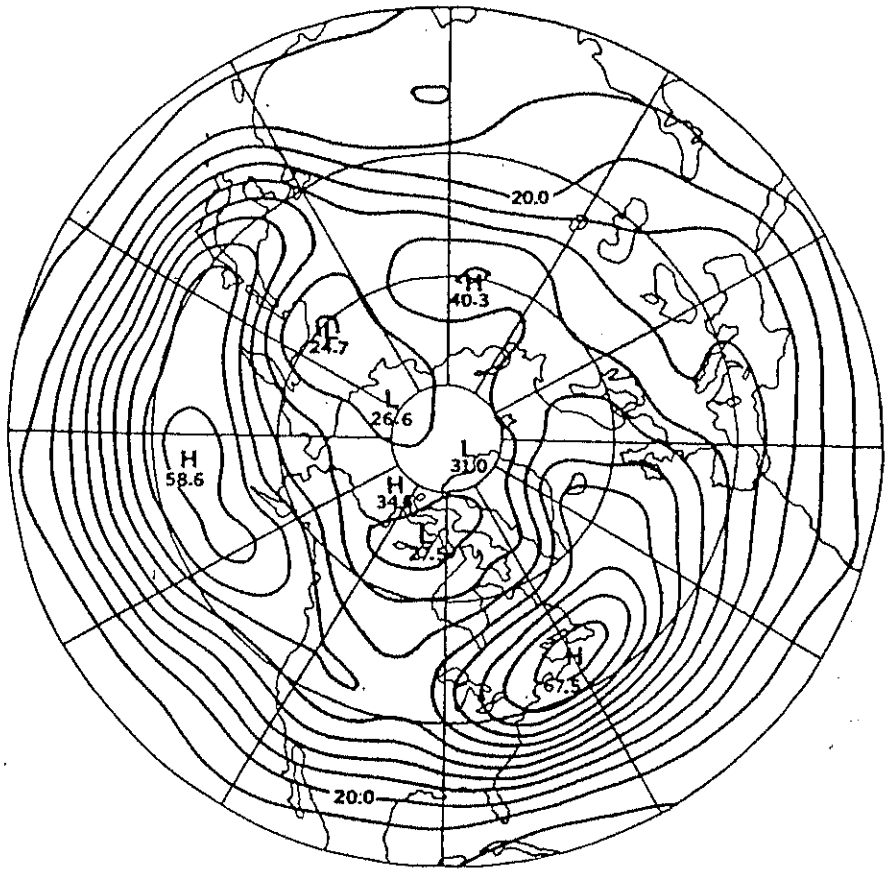

(a)

FIGURE 11. RMS deviation of the winter 500-mb bandpass geopotential height field in the Northern Hemisphere (units of m, contour interval is 5 m): (*a*) observed winter; (*b*) GCM winter.

From such studies as just discussed, we conclude the following:

(a) GCMs show a remarkable degree of success in simulating the geographical location, intensity, and life cycle of synoptic scale disturbances, as inferred from the similarities in observed and model-simulated bandpass filtered height variances. The geographical locations of the storm tracks in relation to mean field structures are also well simulated.

(b) GCMs do not simulate as well the low-pass filtered variance. The amplitudes are less in every model and sometimes even the geographical locations are not well simulated. Since the maxima in low-pass variance are coincident with the maxima in the frequency of blocking in all seasons

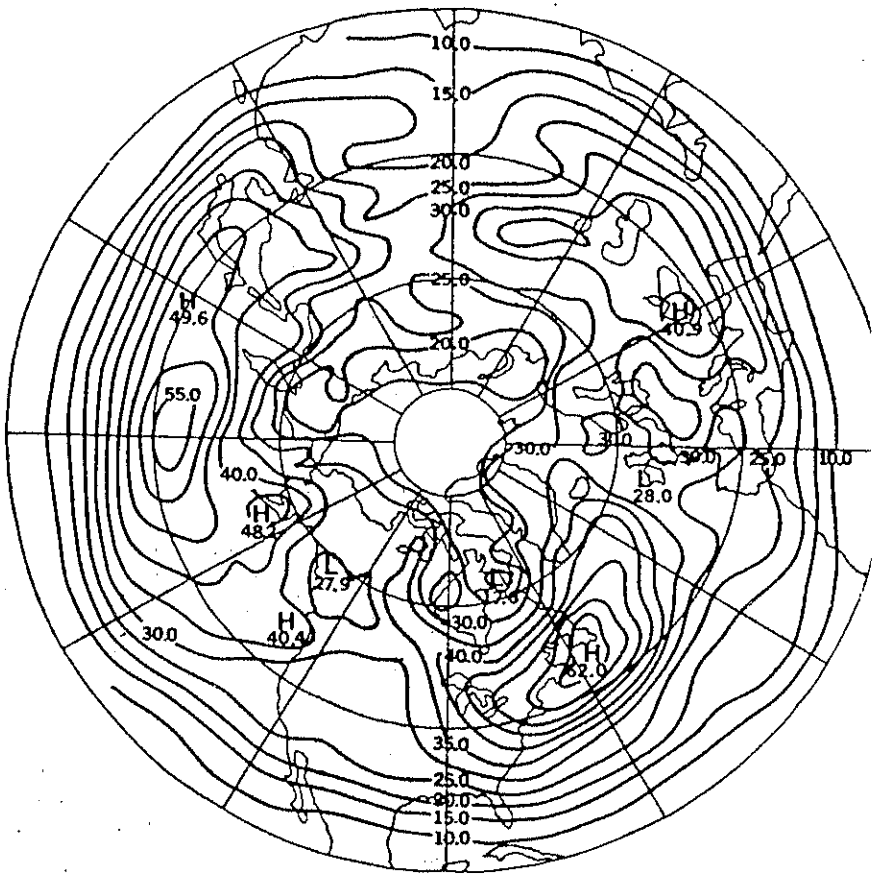

(b)

FIGURE 11. (*continued*)

(Shukla and Mo, 1981; Dole, 1982) it is unlikely that the models will simula the amplitude, location, and duration of observed blocking events correctl

Simulation of Blocking

The midlatitude atmospheric flow pattern is occasionally dominated b quasi-persistent features whose time scale is larger than the life cycle individual storms but shorter than the length of a season. These feature generally referred to as blocking, are of great importance to medium-ran and monthly prediction. Shukla and Mo (1981) and Dole (1982) have e amined the geographical and seasonal occurrences of persistent anomali in the geopotential height field over the Northern Hemisphere. They four that large positive anomalies (>100–200 m) persist at three distinctly di

ferent geographical locations: from the Pacific to the west of the Rockies, from the Atlantic to the west of the Alps, and from the Scandinavian mountain ranges to the west of the Ural Mountains of the USSR. The local structure of blocking in all three regions is very similar, and these preferred locations do not change with season.

A preliminary analysis of climatology of blocking in the GLAS climate model is presented by Shukla et al. (1981b). They examined 17 winter and 7 summer short-term simulations to determine the frequency and geographical locations of the model-simulated blocking events. A blocking event was identified at any grid point that a 500-mb geopotential height anomaly (departure from the mean seasonal cycle) of 100 gpm or more persisted for 7 days or more. The geographical locations of the maximum blocking events were not in good agreement with observed locations. The model underestimated the intensity of blocking ridges. Several blocking features appeared, but they did not persist with amplified magnitude. Chen and Shukla (1983) have analyzed a strong blocking situation, the strongest that was simulated by the GLAS climate model, which occurred in a winter simulation with large sea surface temperature (SST) anomalies in the northern Pacific such as observed during January 1977. Mansfield (1981) and Gilchrist (1982) have also examined the blocking situations in the British Meteorological Office GCM. Some of the factors that affect the location, intensity, and duration of blocking events in a GCM are described below.

Resolution

If the maintenance of the blocks were due to interactions between the large-scale circulation and small-scale waves, and if the model resolutions were not adequate to resolve the latter and their interactions with the former, the inadequate resolution might be one of the causes for unrealistic simulation. Examination of blocking in high-resolution models could shed further light on this matter.

Structure of Zonal Flow

Tung and Lindzen (1979) have suggested that the vertical structure of zonal winds, especially at higher levels, is very important for setting up stationary waves and blocking. Since most of the models do not simulate the zonal winds and temperatures at the higher levels, they may not produce realistic blocking events either.

Diabatic Heat Sources

If some of the observed blocking events were due to either the influence of anomalous midlatitude stationary thermal forcings (because of anomalies of SST, snow, or sea ice, etc.) or to tropical heat sources (because of anomalies of SST or soil moisture), the models would not be able to simulate them because they use climatological boundary forcing. We do not understand the precise role of slowly varying boundary forcing in the generation and

maintenance of blocking events. Possibly, although the large-scale qua stationary flow patterns are initiated by stationary forcing, the small-sc waves and their interactions may be important for the maintenance of t blocks.

Even in the absence of quasi-stationary thermal forcing, blocks may generated by interactions between fluctuating zonal winds and mounta (Charney and Devore, 1979; Charney and Straus, 1980; Charney et al., 198 and in this context, lack of GCM's ability to simulate blocking can be tributed to inadequate treatment of interactions between the zonal flow a orography. The apparent regional nature of the blocking and locally amplifi ridges could be due to the longitudinal variations of zonal flow (an opini of the late Professor Charney), which are in turn caused by the longitudi variations of diabatic heating. If GCMs were not able to simulate the h sources and the asymmetric zonal flows, they would also be deficient simulating the blocking events. A more thorough analysis of blocking ph nomena in GCM simulations could clarify the mechanisms of blocking GCMs.

Lau (1981) has shown that the so-called Pacific/North American patte of monthly mean height anomalies is present in a simulation without S anomalies. This does not necessarily mean that the SST anomalies are n important for blocking, because the Pacific/North American pattern is n the same as blocking. D. Gutzler AER (personal communication) has shov that the Pacific/North American pattern can be found even if all the da identified as blocking were removed from the data set before the calculatio for the pattern were made.

INTERANNUAL VARIABILITY OF MONTHLY, SEASONAL, AND ANNUAL MEANS

The interannual variability of the time mean or transient circulation consis of two parts: that due to the internal dynamics with prescribed seasonal varying boundary forcing and that due to the interannual variability of boun ary forcing itself. The boundary conditions of SST, soil moisture, snow, s ice, and so on can be prescribed to have their mean seasonal variation, an GCMs can then be integrated for several years to calculate the interannu variability due to internal dynamics. Similarly, GCMs can be integrated wi time-varying (interannually as well as seasonally) boundary forcing to d termine the total interannual variability due to the combined effects of i ternal dynamics and boundary forcing. To our knowledge, neither of th above two integrations has been performed with any large complex GC for a simulated time period of 10 y or more. The model simulation of Manab and Hahn (1981) is a hybrid of both approaches. Manabe and Hahn pr scribed the seasonally varying (but not interannually varying) SST but a lowed the soil moisture and snow cover to vary interannually as determine

by the model parameterizations. We shall describe their results in the next section.

GFDL Spectral Model Results for a 15-Year Integration

Manabe and Hahn (1981) have presented the results of a simulation of atmospheric variability from the last 15 y of a 17.75-y integration of the GFDL spectral climate model. The description of the model and simulation of mean fields is given in Manabe et al. (1979). Sea surface temperature, cloud amounts, insolation, and ozone are prescribed for each calendar day of the year and have no interannual variability; therefore, the simulated interannual variability is mainly due to internal dynamics and changes in snow cover and soil moisture. This simulation has been examined further by Lau (1981) to study recurrent meteorological anomalies.

The studies find that the geographical structure of the simulated variability of daily and monthly means is in good agreement with the observations. The magnitude of the variability is systematically underestimated in the tropics and is either comparable to or less than is observed in the middle latitudes. In the regions of systematic underestimation of simulated sea level pressure, daily and monthly variability is overestimated. According to Lau (1981), the rms amplitude of 500-mb monthly mean heights is about 70–80% of that observed in the atmosphere. They have not presented results of interannual variability of seasonal means.

Figure 12*a* shows the zonal means of observed and simulated standard deviation of daily and monthly mean 1000-mb geopotential height (m) for the December–February season. The model systematically underestimates the observed variability in the tropics. As the averaging period increases from one day to one month, the model-simulated tropical variability decreases further. For example, at the equator, the model variability is ~70% of the daily and only about 45% of the monthly observed variability. It is likely that most of the monthly variability in the model is due to the sampling of daily values, which have rather large autocorrelation decay times of 4–8 days (see Figure 5.13 of Manabe and Hahn 1981). The interannual variability of simulated seasonal means was probably also too low in the tropics.

Figure 12*b* shows latitude–pressure distributions of the zonal mean standard deviation of the monthly mean geopotential height (m) for the December–February season. Although the extratropical variability is underestimated only slightly, the simulated tropical variability in the upper troposphere and stratosphere is smaller by factors of 2 and 3, respectively.

The ratio of the observed to simulated standard deviation of Northern Hemisphere mean surface air temperature is about 1.8 for daily, 2.0 for 3 month running means, and 3.0 for 12-month running means. It is not clear whether this difference is genuine or just a result of differences in sampling of observed and model-simulated data.

The first eigenvector of the normalized monthly mean 500-mb height field

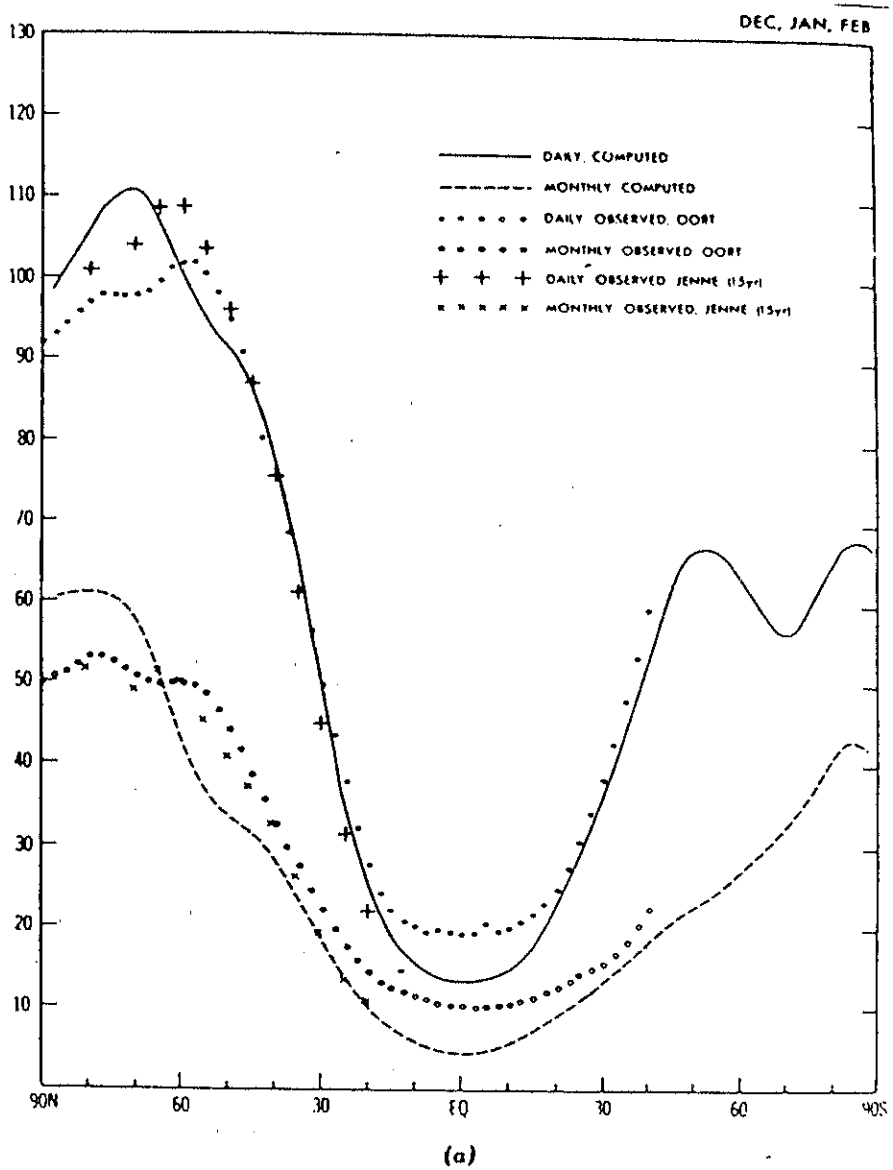

FIGURE 12. Zonal means of standard deviation for December–February season for: (*a*) daily and monthly mean 1000-mb geopotential height; (*b*) latitude–pressure distribution for monthly mean geopotential height (m). [From Manabe and Hahn (1981) with permission of *Monthly Weather Review*, the American Meteorological Society.]

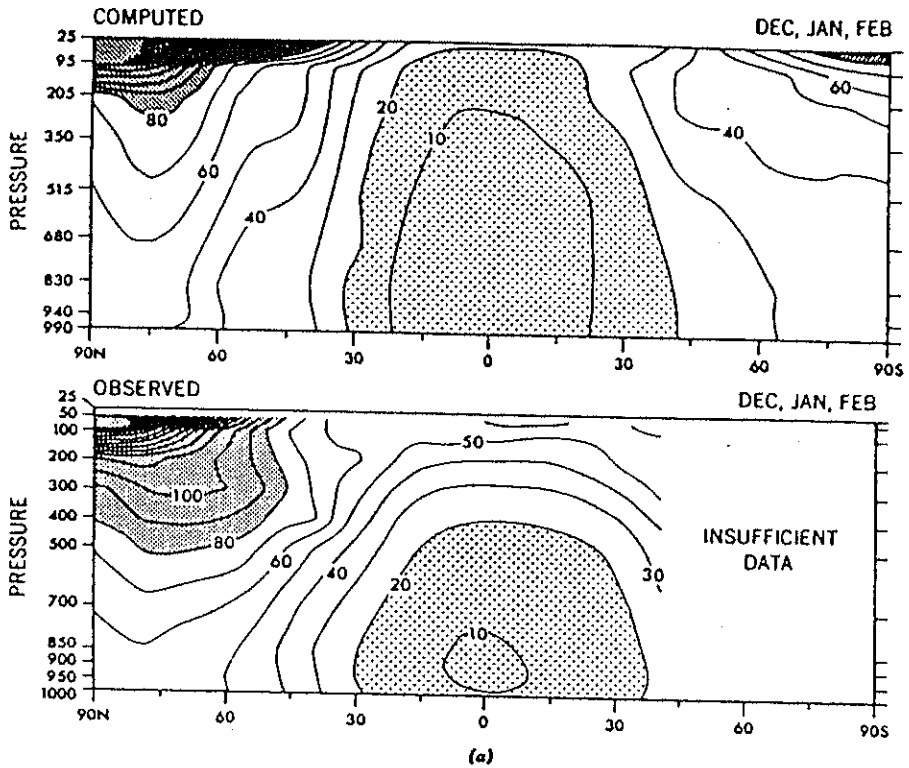

(a)

FIGURE 12. ***(continued)***

for winter looks similar to the corresponding eigenvector from observations, although there are some differences in the locations and amplitudes of anomaly centers. The model-simulated first eigenvector explains 22.4% of the hemispherically integrated variance.

Thus, even in the absence of variable SST anomalies, large-scale, though poorly understood fluctuations do occur in the model atmosphere. The basic mechanisms for such fluctuations could involve the interactions of fluctuating zonal winds with orography, the instability of the three-dimensional flow, or the tropical and midlatitude transient diabatic heat sources associated with episodes of enhanced or reduced precipitation caused by the internal dynamics itself. A more detailed analysis of the model-simulated rainfall is needed in order to investigate the possible role of tropical heat sources in causing these large-scale fluctuations.

Figure 13 shows the structure of the first eigenvector of the normalized monthly mean geopotential height at (a) 300 and (b) 1000 mb for all 12 months of the year over the tropics. The most conspicuous features are the lack of zonal variation and a complete absence of any signature of the southern

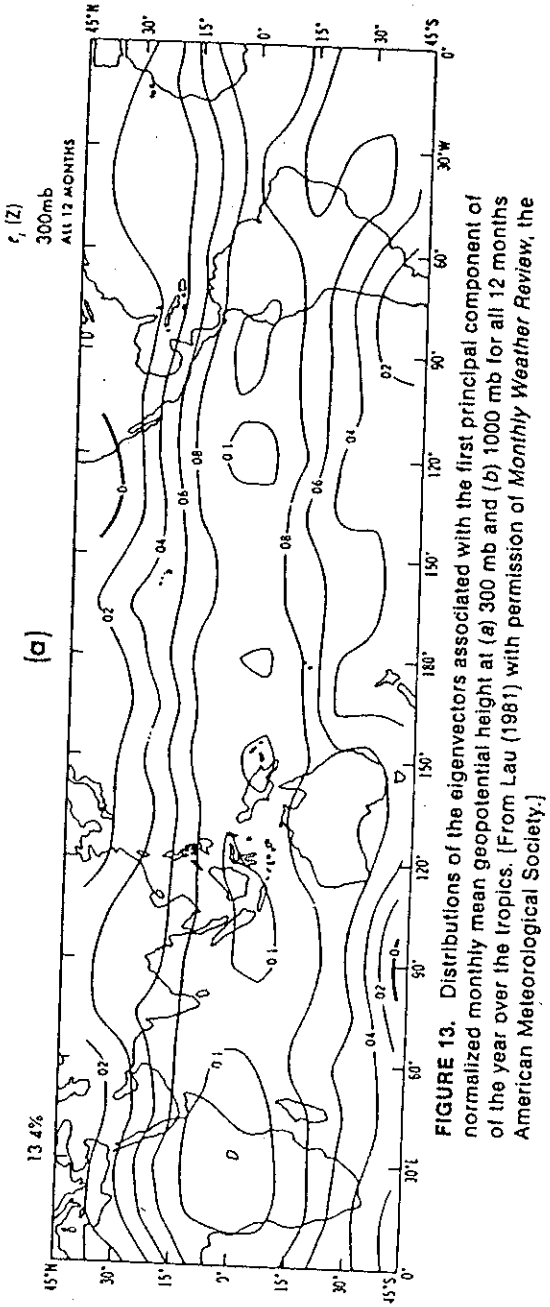

FIGURE 13. Distributions of the eigenvectors associated with the first principal component of normalized monthly mean geopotential height at *(a)* 300 mb and *(b)* 1000 mb for all 12 months of the year over the tropics. [From Lau (1981) with permission of *Monthly Weather Review*, the American Meteorological Society.]

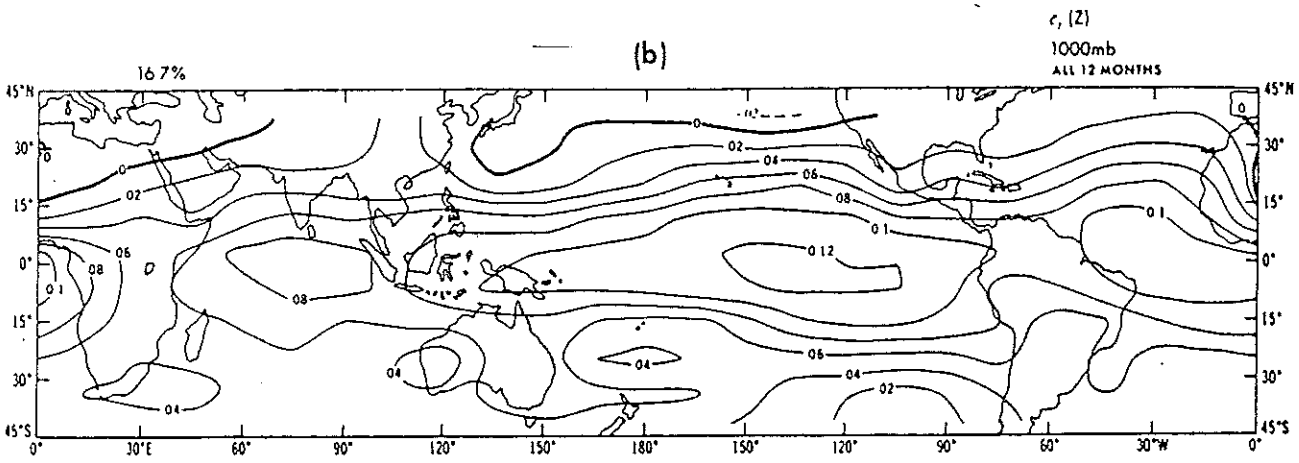

FIGURE 13. (*continued*)

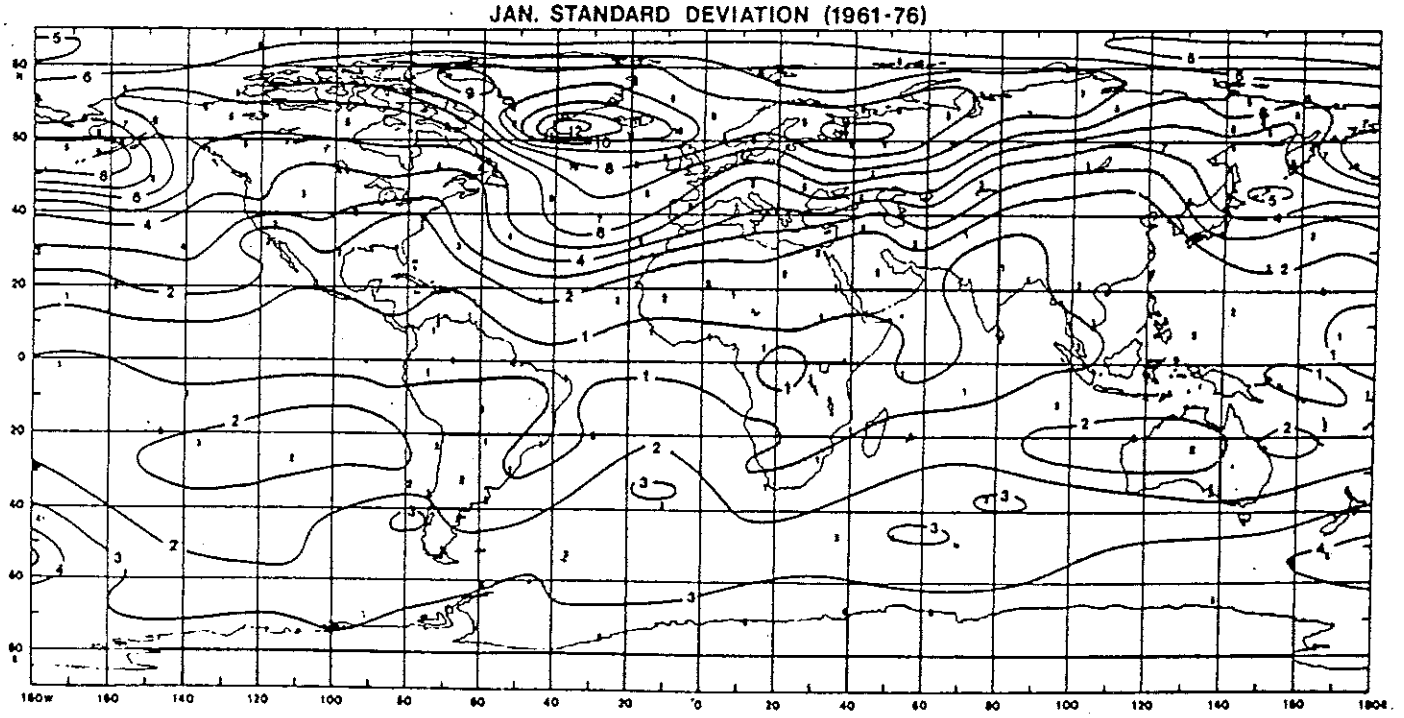

(*a*)

FIGURE 14. Standard deviation of monthly mean sea level pressure (mb): (*a*) observed January (Godbole and Shukla, 1981); (b) GCM February [from Shukla (1981a) with permission of *Journal of the Atmospheric Sciences*, the American Meteorological Society].

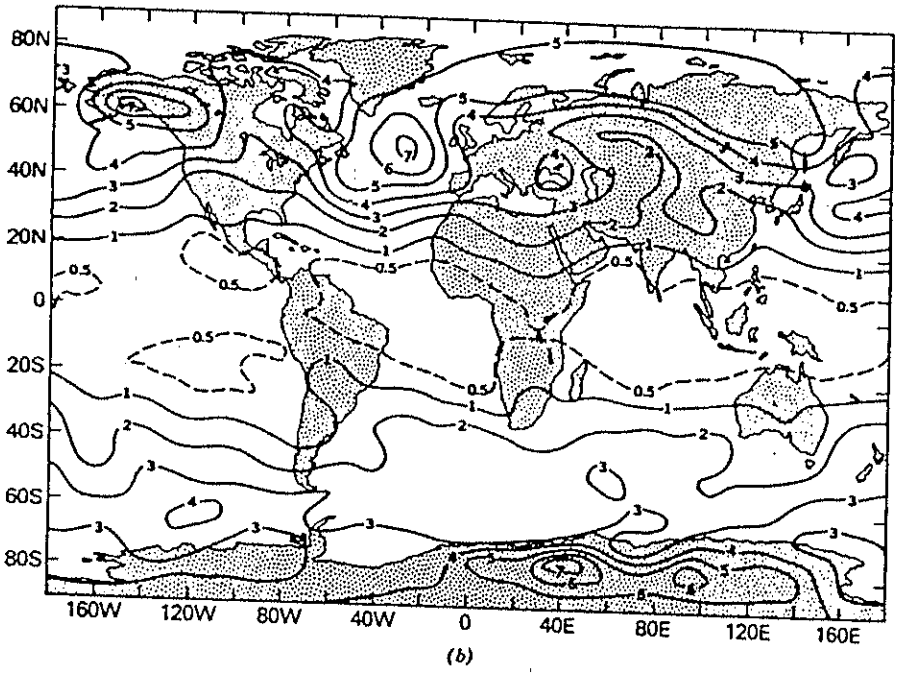

(b)

FIGURE 14. (*continued*)

oscillation (not shown), which would give opposite signs over the Indian Ocean and the eastern tropical Pacific. According to Lau (1981), the pattern based on simulated winter data alone is very similar to the one shown here, and the next few eigenvectors also do not show any signature of the southern oscillation.

Simulations with Different Initial Conditions

Shukla (1981a) integrated the GLAS climate model for 60 days with nine different initial conditions but identical boundary conditions. Three of these initial conditions were the observed atmospheric conditions on January 1 of 1975, 1976, and 1977, and six other initial conditions were obtained by superimposing over the observed initial conditions a random perturbation for which the rms error for all the grid points was 3 m s^{-1} in u and v components of wind. Figure 14*b* shows the global map of standard deviation of the nine monthly means for the second month (February) of the model integration. Figure 14*a* shows the standard deviation of the observed monthly mean sea level pressure for 16 y (1961–1976) from Godbole and Shukla (1981). The model-simulated variability is uniformly smaller than the observed variability. This difference is partly due to the absence of anomalous boundary forcing and partly due to the limited duration of the model integrations, which

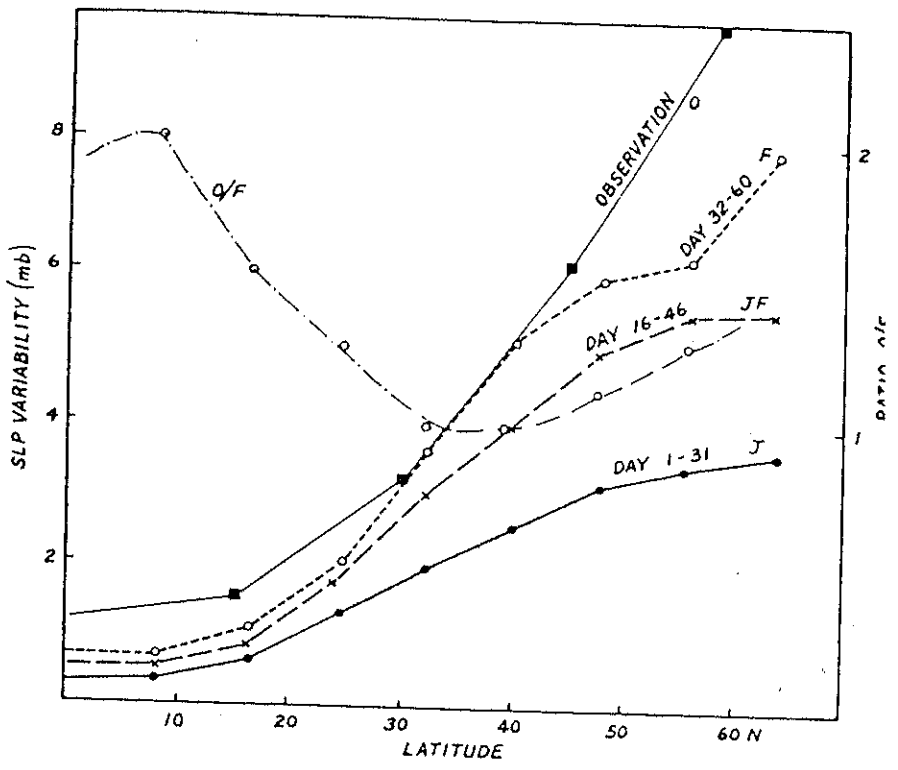

(a)

FIGURE 15. (*a*) Zonally averaged rms deviation of sea level pressure (mb) between contro and perturbation runs averaged for days 1–31, 16–46, and 32–60 (O/F = ratio of obser vations and model for days 32–60). (*b*) Zonally averaged standard deviation of daily gri point values for sea level pressure (mb) for January (upper panel) and February (lowe panel) for model (solid line) and observations (dashed line). [From Shukla (1981a) wit permission of *Journal of the Atmospheric Sciences*, the American Meteorological Society.

does not allow very low frequency internal dynamical processes to affec the monthly means. Figure 15*a* shows the zonally averaged standard devia tions for observed and model-simulated monthly mean sea level pressure and the ratio of observed-to-simulated zonally averaged standard deviations. The ratio is about 2 in the low latitudes and about 1 in the middle latitudes. Figure 15*b* shows the zonally averaged daily standard deviations of sea level pressure for observations and model simulations, which are in good agreement.

Figure 16*b* shows the standard deviation of model-simulated monthly mean rainfall (mm day^{-1}) for February, and Fig. 16a shows the observed standard deviation of mean rainfall (cm $month^{-1}$) for the winter season over land for 16 y (1963–1976). Although the general pattern of the simulated standard deviations (locations of large maxima and minima) shows some

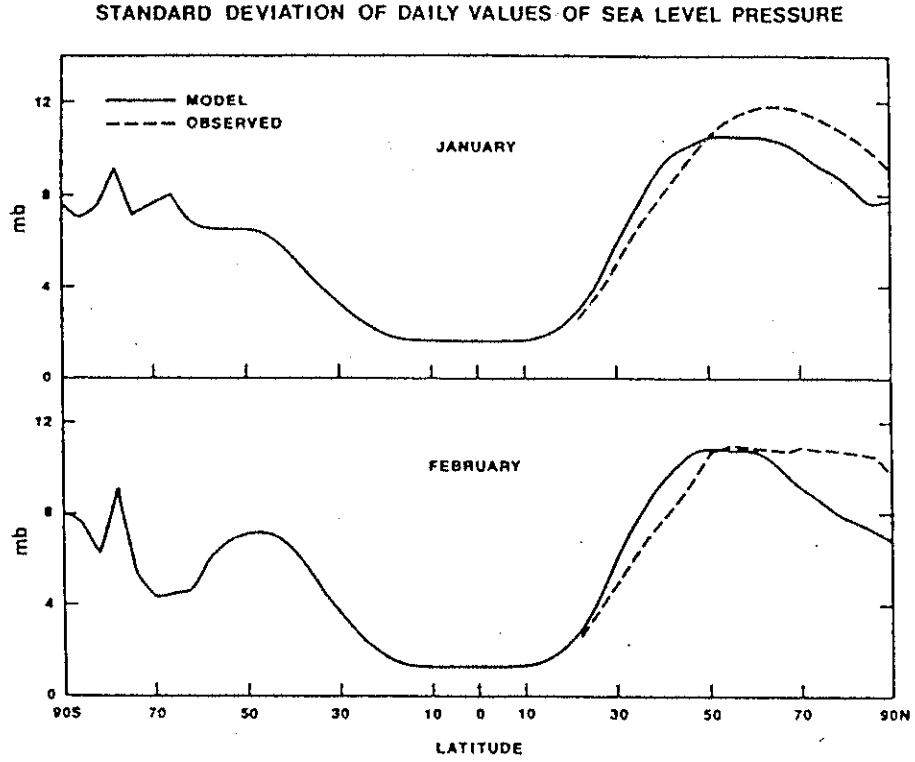

(b)

FIGURE 15. (*continued*)

similarity to the observations, the magnitudes, especially in the tropics, are clearly underestimated. Evidently, interannual variability of boundary forcing is quite important for the interannual variability of monthly and seasonal mean rainfall.

Charney and Shukla (1981) examined the variability of the monthly mean (July) circulation for four model runs for which the boundary conditions were kept identical but the initial conditions randomly perturbed. Although the observed and model variabilities were comparable at middle and high latitudes, the variability among the four model runs for the monsoon region was far less than the observed interannual variability of the atmosphere, possibly because of fixed boundary conditions. Manabe and Hahn (1981) gave a similar explanation for the model-simulated low variability in the tropics. However, for inferring such conclusions about the role of boundary forcing, it is more appropriate to make integrations with and without the influence of the boundary forcing, so that two properties of the same model can be directly compared and any intrinsic model deficiency will not bias

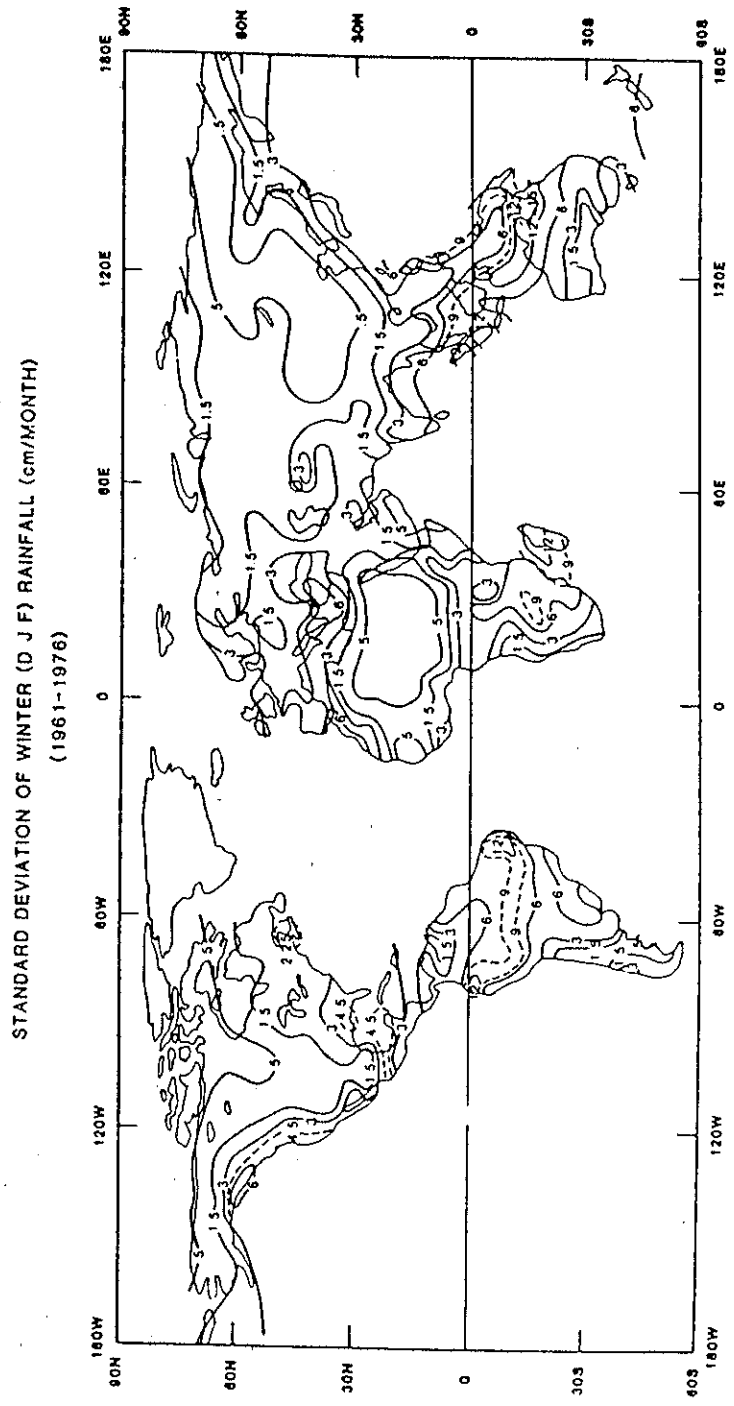

(a)

FIGURE 16. Standard deviation of (*a*) observed seasonal mean rainfall (cm month^{-1}) based on 16 years (1962–1977) and (*b*) GCM February mean rainfall (mm day^{-1}) for nine model runs (Shukla, 1981a).

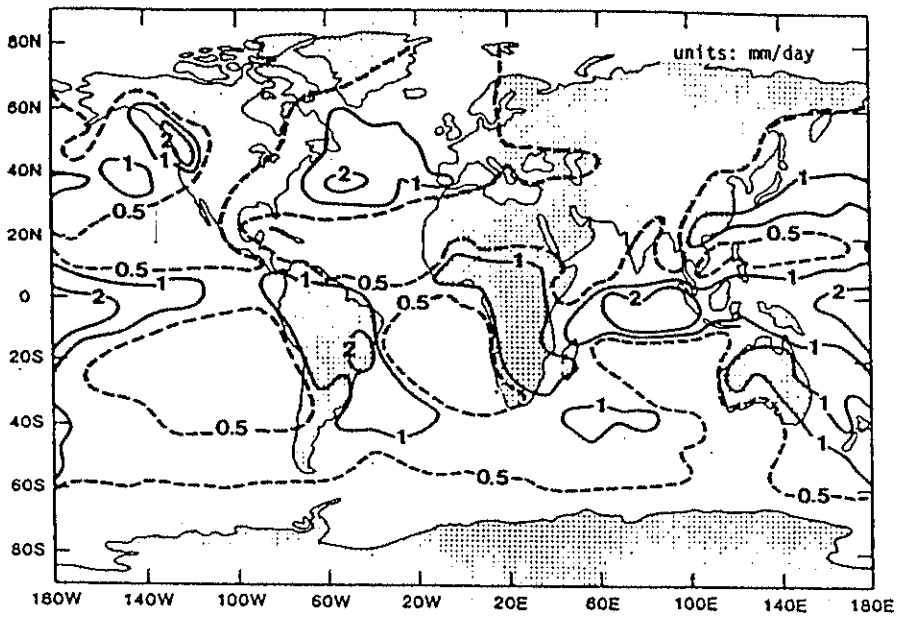

(b)

FIGURE 16. (*continued*)

the results. The results of a preliminary study along these lines by Shukla (1981b) are summarized below.

Effect of Different Sea Surface Temperature Distributions

The GLAS climate model was integrated for 45 days starting from the observed initial conditions in the middle of June and with climatological mean boundary conditions [referred to as the control (C) run]. Three additional integrations for 45 days were done by randomly changing the initial conditions of u and v at each of the nine model levels but retaining the same boundary conditions. The random errors corresponded to a Gaussian distribution with zero mean and a standard deviation of 3 m s^{-1} for u and v separately. These integrations are the predictability (P_1, P_2, P_3) runs. Three additional integrations for 45 days were made in which, in addition to randomly perturbed initial conditions, the boundary conditions of SST between the equator and 30°N were replaced by the observed SST during July of 1972, 1973, and 1974. These integrations are the boundary forcing (B_1, B_2, B_3) runs. The variance (σ_p^2) among monthly means of C, P_1, P_2, and P_3 gives a measure of the natural variability of the model, that is, the variability caused by internal dynamics alone. The variance (σ_B^2) among monthly means of C, B_1, B_2, and B_3 gives a measure of the variability including

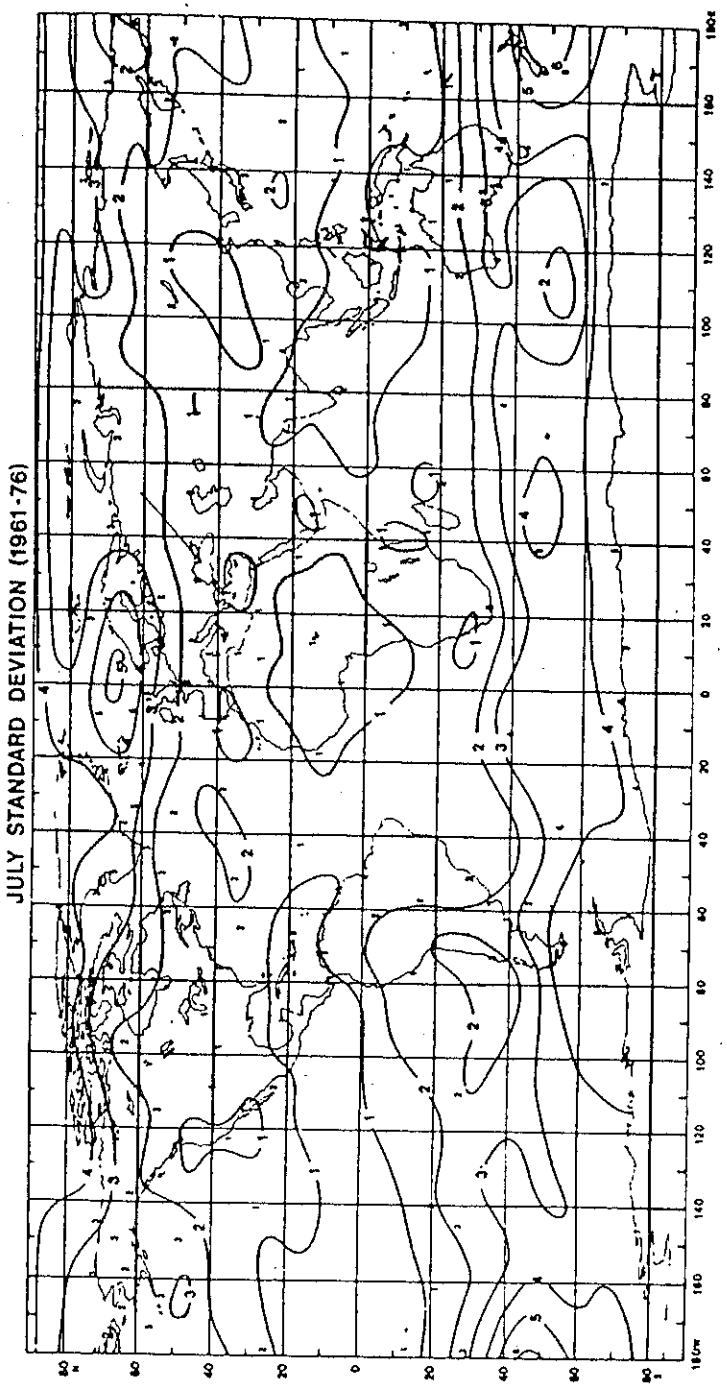

(a)

FIGURE 17. Standard deviation of monthly mean sea level pressure (mb): (*a*) observed July (Godbole and Shukla, 1981); (*b*) GCM July (Shukla, 1981b)

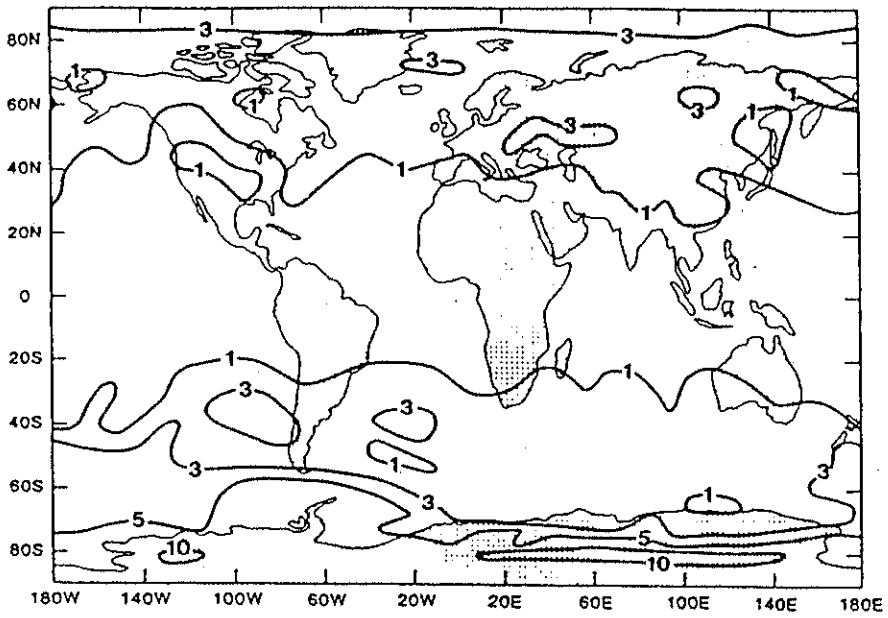

(b)

FIGURE 17. (*continued*)

boundary forcing of SST. We have compared σ_p and σ_B with the observed standard deviation (σ_o) for 10 y of monthly means. Figure 17 shows the global maps of σ_o and σ_p. The July standard deviation fields for the model are considerably smaller than is observed, with the most pronounced discrepancy occurring in the tropics.

Figure 18*a* shows plots of zonally averaged values of σ_p, σ_B, and σ_o and the ratios σ_o/σ_p and σ_p/σ_B. In agreement with the results of Charney and Shukla (and Manabe and Hahn), the ratio σ_o/σ_p is more than 2 in the tropics and close to 1 in the middle latitudes. The ratio σ_B lies nearly halfway between σ_o and σ_p, which suggests that nearly half of the remaining variability was accounted for by changes in SST between the equator and 30°N. The influence of other variable boundary forcing by soil moisture or snow cover would further bring σ_B closer to σ_o. These results, although for short period integrations, are in remarkable agreement with those of Manabe and Hahn, which are based on 15 y of model integration. We have calculated the ratio σ_o/σ_M (where σ_M refers to model-simulated standard deviations) from the two curves of Manabe and Hahn (shown in Fig. 12*a* of this essay) and the results are shown in Fig. 18*b*. The ratio σ_o/σ_M is again about 2 in the near equatorial regions and is reduced to about 1 in the middle and high latitudes. The corresponding ratio for the height field in the tropical troposphere and stratosphere is more than 3 (see Fig. 12*b*).

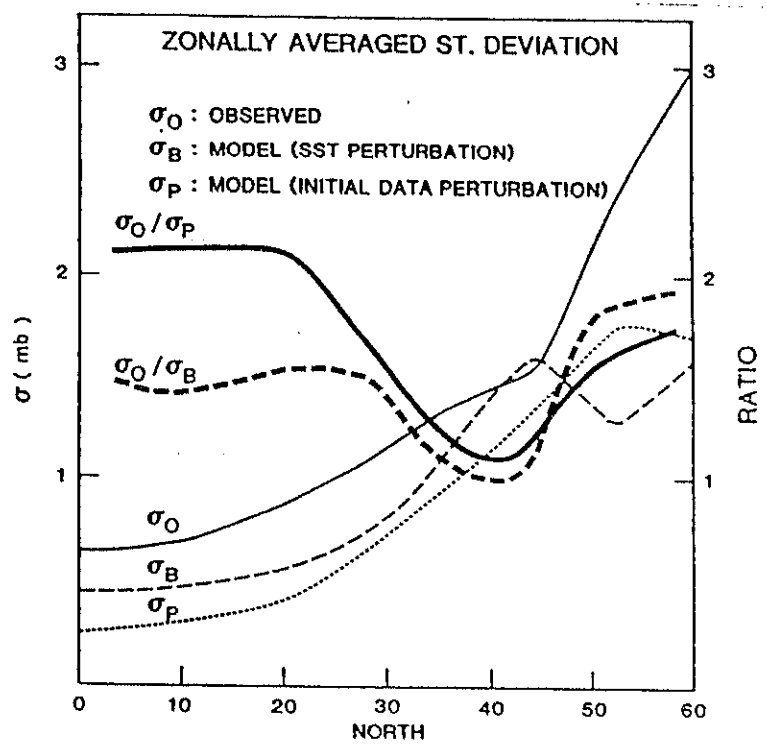

(a)

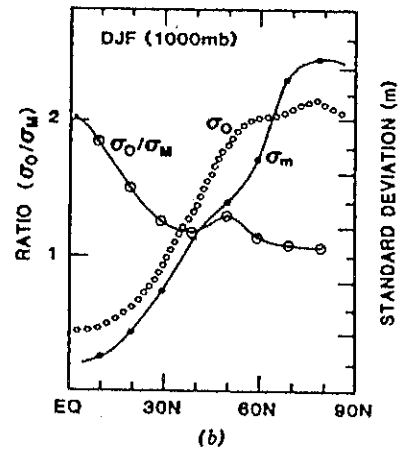

(b)

FIGURE 18. (*a*) Zonally averaged standard deviation among monthly mean (July) sea level pressure (mb) for 10 y of observations (σ_o, thin solid line); four model runs with variable boundary conditions (σ_B, thin dashed line); and four model runs with identical boundary conditions (σ_p, thin dotted line). Thick solid line and thick dashed line show the ratio σ_o/σ_p and σ_o/σ_B, respectively. (*b*) Zonal means of standard deviation of monthly mean 100 mb geopotential height (m) from Manabe and Hahn (1981). On the left side is the ratio (σ_o/σ_m) of observed and model standard deviations.

The additional variability explained by ocean temperature variations, taken together with the analysis of Lau (1981), which showed that the southern oscillation was not simulated by the model simulations of Manabe and Hahn, suggests that the slowly varying boundary forcings are the most important mechanisms for determining the interannual variability of the monthly and seasonal means in the tropics. However, more systematic GCM simulation studies with and without boundary forcing are needed to understand better the relative importance of internal dynamics and boundary forcing and whether or not tropical boundary forcing can also influence the simulation of midlatitude variability.

A recent paper by Lau (1985) is a good example of work in this direction. Using the observed SST in the tropical Pacific for a 15-y integration of a GFDL spectral model, he has shown that the interannual variability of the southern oscillation is simulated rather well. Correlation coefficients between the prescribed SST anomalies in the tropical Pacific and midlatitude circulation over the Northern Hemisphere are also in good agreement with the observations.

INTERANNUAL VARIABILITY OF INTRASEASONAL SPACE–TIME FLUCTUATIONS

The interannual variability of model-simulated intraseasonal space–time fluctuations has yet been little studied. Figure 17 in Lau (1981) is the only such result that we could find. Lau presents composite charts of rms of bandpass filtered 500-mb height for five simulated winter seasons that had large positive amplitudes of the first eigenvector of normalized monthly mean 500-mb height and compared it with a composite of another five winter seasons that had large negative amplitude of the same eigenvector. He found that the displacements of maxima of bandpass filtered rms (which represent storm tracks) are consistent with shifts in large-scale circulation features such as the location of jet streams and regions of enhanced baroclinicity.

PREDICTABILITY OF TROPICAL ATMOSPHERE

The large-scale time-mean tropical atmosphere is potentially more predictable than the extratropical atmosphere, because its planetary-scale circulations are dominated by Hadley, Walker, and monsoon circulations, which are intrinsically more stable than is the midlatitude Rossby regime. Interaction of these large-scale overturnings with tropical disturbances (easterly waves, depressions, cyclones, etc.) is not strong enough to make the former unpredictable because of the unpredictability of the latter.

Tropical disturbances are initiated by barotropic–baroclinic instabilities, but their main energy source is the latent heat of condensation. Although

their growth rate is fast and they are deterministically less predictable than midlatitude disturbances, their amplitude equilibration is also quite rapid and they attain only moderate intensity.

The intensity and geographical location of Hadley and Walker cells are primarily determined by the boundary conditions and not by synoptic-scale disturbances. Thus, frequency and tracks of depressions and easterly waves are likely controlled by the location and intensity of Hadley and Walker cells and by the distribution of SST and soil moisture fields. It is unlikely that details of tropical disturbances have much influence on the large-scale tropical circulation. By contrast, in midlatitudes, synoptic-scale instabilities interact with planetary-scale circulations to such an extent as to make them less predictable. The circulation in midlatitudes consists of baroclinic waves, long waves, and planetary waves of different wave number and frequency, whereas in the tropics the circulation is clearly separated between the large-scale Hadley and Walker cells and the synoptic-scale disturbances. In other words, tropical spectra in space, as well as in time, are redder than are midlatitude spectra.

The interannual variability of the seasonal mean tropical circulation and rainfall results largely from changes in the location and intensity of the thermally driven Hadley and Walker circulations (Moura and Shukla, 1981). Although the reasons for the positions and intensities of the climatological mean rainfall maxima (corresponding to the ascending branches of Hadley and Walker cells) are not well understood, it appears that the interannual fluctuations of these thermally driven circulations are closely related to the changes in the boundary conditions (viz. SST and soil moisture) at the earth's surface. Much of the local interannual variability over different parts of the tropics is in fact a regional manifestation of the planetary-scale El Niño–southern oscillation–monsoon phenomena resulting from interactions among the atmosphere, the oceans, and the land processes. Some of the largest anomalies in circulation and rainfall, comprising a major portion of the interannual variability, are strongly phase locked with the seasonal cycle. Thus, the major tropical droughts and floods are due either to an amplification of the annual cycle or to shifts in the locations of maximum amplitude.

Atmosphere–Ocean Interactions

The winter of 1982–1983 witnessed the most outstanding example of large persistent SST anomalies over the equatorial Pacific and related circulation anomalies over many parts of the globe. Since the influence of tropical SST anomalies on atmospheric circulation, locally as well as globally, may be important for prediction of short-term climate, we should understand the mechanisms through which SST anomalies influence the atmospheric circulation. Several climate modeling groups have conducted sensitivity experiments for tropical Pacific SST anomalies using their respective GCMs (Blackmon et al., 1983; Shukla and Wallace, 1983). During the Sixteenth

Liège Colloquium on Hydrodynamics (May 1984), a session was devoted to intercomparison of the results from the various modeling groups.

Papers were presented by the following authors reporting on the GCMs of the listed institutions: M. Blackmon, National Center for Atmospheric Research; G. Boer, Canadian Climate Center; V. Cubash, European Centre for Medium Range Weather Forecasts; S. Esbensen, Oregon State University; M. Fennessy, L. Marx, and J. Shukla, Goddard Laboratory for Atmospheric Sciences; A. Oort and N. C. Lau, Geophysical Fluid Dynamics Laboratory; T. N. Palmer and D. Mansfield, British Meteorological Office; R. Sadourny and R. Michaud, Laboratoire de Météorologie Dynamique; and M. Suarez, University of California, Los Angeles.

All the models correctly simulated the general eastward shift of the rainfall maximum over the central equatorial Pacific but with some quantitative differences. The consistency of the results using such widely different GCMs confirmed the earlier hypothesis that tropical SST anomalies can produce significant and predictable changes in tropical rainfall and circulation. Similarities among the simulations of the midlatitude response were not so obvious.

We shall present here, as an example, a sensitivity study with the GLAS climate model using the observed SST anomalies over the tropical Pacific during the winter of 1982–1983 (Fennessy et al., 1985). Figure 19 (top panel) shows the observed SST anomaly during January 1983, which was added to the climatological SST with the model integrated for 60 days. This integration is referred to as the *anomaly run*, and a similar integration with climatological SST is referred to as the *control run*. Such pairs of integrations were made for three different initial conditions. Figure 19 also shows the difference in precipitation between the anomaly and control runs averaged for these three pairs for the period of days 11–60 (middle panel) and the rainfall anomaly calculated from the observed outgoing long-wave radiation for the 1982–1983 winter (bottom panel). The outgoing long-wave radiation anomalies are converted to rainfall anomalies using empirical relations. It is remarkable that the model calculations have been able to simulate the location as well as the intensity of the rainfall anomaly rather well.

To study the role of tropical SST anomalies, Lau and Oort (1984) and Lau (1985) examined a 15-y integration of the GFDL model with the observed SST anomalies over the equatorial Pacific. In the simulation without the SST anomalies (Lau, 1981), there was no evidence for the planetary-scale seesaw of surface pressure referred to as the southern oscillation, which is one of the most dominant modes of tropical variability, whereas in the simulation with the SST anomalies, the southern oscillation is simulated remarkably well. The observed correlations between the tropical SST anomalies and midlatitude circulation are also simulated remarkably well in the 15-y simulation with the SST anomalies.

Philander and Seigel (1985) and Latif (1985) have shown that realistic simulation of oceanic circulation and SST anomalies in tropical oceans can

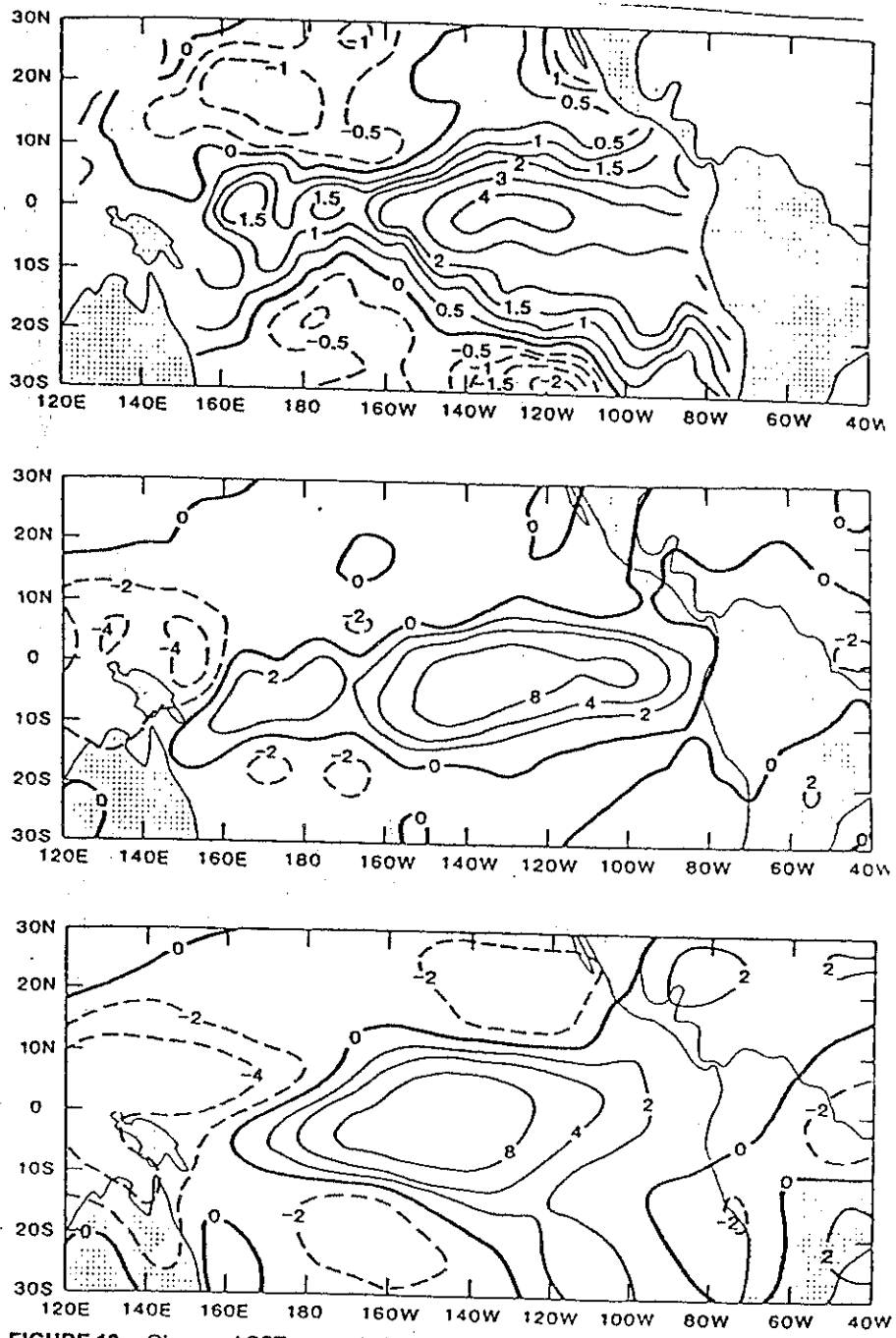

FIGURE 19. Observed SST anomaly (°C) for January 1983 (*top*), model-simulated rainfall (mm day^{-1}) (*middle*), and observed rainfall anomalies (*bottom*).

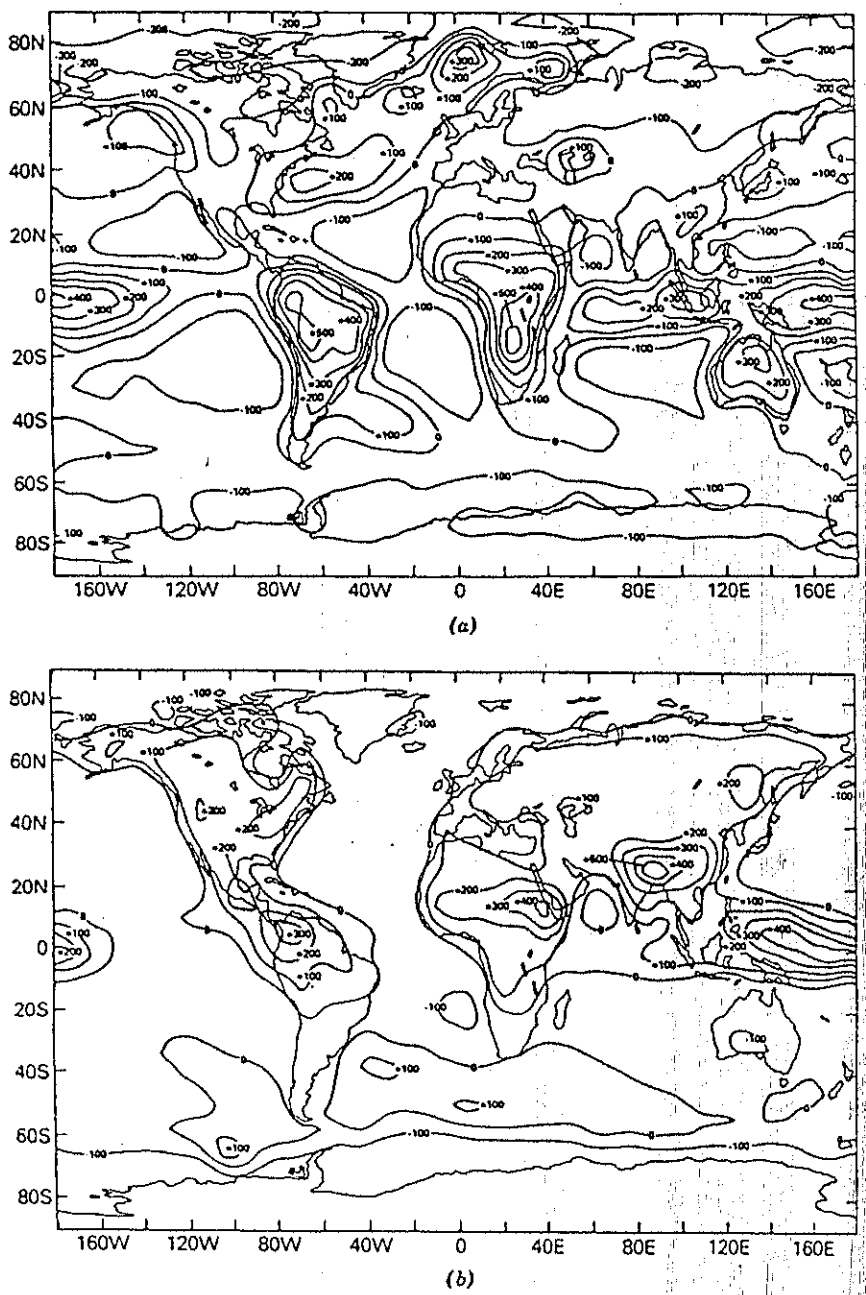

FIGURE 20. (*a*) Vertically integrated net diabatic heating (cal cm^{-2} day^{-1}) of the atmosphere during winter, as simulated by the GLAS climate model. (*b*) Vertically integrated net diabatic heating (cal cm^{-2} day^{-1}) of the atmosphere during summer, as simulated by the GLAS climate model.

be obtained by using the prescribed wind stress from the atmospheric observations. These results of one-way forced ocean models are quite encouraging and suggest that the predictability of the coupled ocean–atmosphere system could be longer than the predictability of the atmosphere alone.

Atmosphere–Land Interactions

Several model sensitivity studies suggest that changes in the land surface boundary conditions influence the tropical circulation on regional as well as on planetary scales (Shukla and Mintz, 1982; Mintz, 1984). Changes in soil moisture, albedo, or vegetation change the partitioning of the incoming radiant energy into sensible and latent heat. Changes in the ground temperature, evaporation, and cloudiness can produce regional effects, but changes in rainfall can produce planetary-scale effects because they represent changes in the deep diabatic heat sources that drive the atmospheric circulation. Although the land surface area is smaller than the ocean surface area, the influence of the land surface forcing functions can be very large because the maxima of the vertically integrated heat sources occur over the land (see Fig. 20*a* for winter and 20*b* for summer), and therefore, for the same fractional change in the intensity of the heat source, the absolute value of the change in the forcing, and consequently the response, may be larger over the land.

FURTHER PROGRESS NEEDED

Although GCMs can realistically simulate the observed large-scale circulation features of summer and winter, some systematic errors remain to be removed. Seasonal cycle simulations still need a detailed analysis of such structural features as seasonal transitions and seasons other than summer and winter. The simulations of low-pass filtered variance and location and intensity and duration of blocking events need further improvement. Interannual variability of model-simulated intraseasonal variability still needs to be examined.

Presumably, the most important mechanism for midlatitude variability is the internal dynamics, while boundary forcing is the most important mechanism for the tropical variability. However, the model integrations necessary to answer these questions still need to be done, as well as further analysis of existing model integrations. We cannot rule out the influence of midlatitude and/or tropical boundary forcing in producing large circulation anomalies in midlatitudes.

Evidently, a significant portion of the variability over different tropical regions is a regional manifestation of the planetary-scale low-frequency disturbances, and major tropical droughts and floods are related to changes in

the amplitude and phase of the annual cycle. Detailed analyses of these connections are still to be developed.

Most of the existing general circulation models do not have an adequate treatment of the physical processes at the land surface, especially the role of vegetation in determining the energy and moisture balance at the earth's surface. These models must be improved before modeling experiments on the impact of regional land surface anomalies would be meaningful. For example, in order to study the impact of deforestation on local and global climate, the model must be integrated first with an adequate treatment of forest. A model climate resulting from deforestation cannot be meaningfully interpreted without a model climate with the forest. The spatial resolution of the models also must be adequate for a description of the physical effects associated with regional changes in land surface properties. In these respects, modeling of atmosphere–land interactions is about 10 y behind the state of modeling of atmosphere–ocean interactions. Several modeling groups are beginning to implement realistic models of the biosphere in general circulation models, and it is hoped that within the next several years there will be systematic numerical sensitivity studies on the effects of changes in land surface conditions and the role of land surface forcing in determining the variability and predictability of the tropical atmosphere.

REFERENCES

Blackmon, M. L., Geisler, J. E., and Pitcher, E. J., 1983. A general circulation model study of January climate anomaly patterns associated with interannual variation of equatorial Pacific sea surface temperatures, *J. Atmos. Sci.* 40, 1410–1425.

Blackmon, M. L. and Lau, N. C., 1980. Regional characteristics of the Northern Hemisphere wintertime circulation: A comparison of the simulation of a GFDL general circulation model with observations, *J. Atmos. Sci.* 37, 497–514.

Blackmon, M. L., Wallace, J. M., Lau, N. C., and Mullen, S. L., 1977. An observational study of the Northern Hemisphere wintertime circulation, *J. Atmos. Sci.* 34, 1040–1053.

Charney, J. G. and Devore, J. G., 1979. Multiple flow equilibria in the atmosphere and blocking, *J. Atmos. Sci.* 36, 1205–1216.

Charney, J. G. and Straus, D. M., 1980. Form-drag instability, multiple equilibria and propagating planetary waves in baroclinic, orographically forced, planetary wave systems, *J. Atmos. Sci.* 37, 1157–1176.

Charney, J. G. and Shukla, J., 1981. Predictability of monsoons, in Sir James Lighthill and R. P. Pearce, Eds., *Monsoon Dynamics*, Cambridge University Press, London, England.

Charney, J. G., Shukla, J., Mo, K. C., 1981. Comparison of a barotropic blocking theory with observation, *J. Atmos. Sci.*, 38, 762–779.

Chen, T. C. and Shukla, J., 1983. Diagnostic analysis and spectral energetics of a

blocking event in the GLAS climate model simulation, *Mon. Wea. Rev.* 111, 3–22.

Dole, R. M., 1982. Persistent anomalies of the extratropical Northern Hemisphere wintertime circulation, Ph.D. Thesis, Massachusetts Institute of Technology, Cambridge, MA.

Fennessy, M. J., Marx, L., and Shukla, J., 1985. General circulation model sensitivity to 1982–83 equatorial Pacific sea surface temperature anomalies, *Mon. Wea. Rev.* 113, 858–864.

Gilchrist, A., 1982. Aspects of the simulation of climate and climate variability in middle latitudes, in *Proceedings of the Study Conference on the Physical Basis for Climate Prediction on Seasonal, Annual and Decadal Time Scales*, Leningrad (USSR), 13–17 September 1982, *World Climate Program Series, WCP-47*, World Meteorological Organization, Geneva, Switzerland.

Godbole, R. V. and Shukla, J., 1981. *Global Analysis of January and July Sea Level Pressure*, NASA Technical Memo. 82097 (NTIS N8124674), Goddard Space Flight Center, Greenbelt, MD.

Halem, M., Shukla, J., Mintz, Y., Wu, M. L., Godbole, R., Herman G., and Sud, Y., 1979. Comparisons of observed seasonal climate features with a winter and summer numerical simulation produced by the GLAS general circulation model, in *GARP Publication Series No. 22*, World Meteorological Organization, Geneva, Switzerland.

Hayashi, Y., 1974. Spectral analysis of tropical disturbances appearing in a GFDL general circulation model, *J. Atmos. Sci.* 31, 180–218.

Hayashi, Y., 1980. Studies of the tropical general circulation with a global model of the atmosphere, in *Proceedings of the Seminar on Impact of GATE on Large-Scale Numerical Modeling of the Atmosphere and Ocean, Woods Hole, Massachusetts, August 20–29, 1979*, National Academy of Sciences, Washington, D.C.

Hayashi, Y. and Golder, D. G., 1980. The seasonal variation of tropical transient planetary waves appearing in a GFDL general circulation model, *J. Atmos. Sci.* 37, 705–716.

Jaeger, L., 1976. Monatskarten des Niederschlags für die ganze Erde, in *Berichte des Deutschen Wetterdienstes*, Vol. 18, No. 139, Offenbach, FRG.

Latif, M., 1985. Western and eastern variability in a model of the equatorial Pacific, Ph.D. thesis, Max-Planck-Institut für Meteorologie, Hamburg, FRG.

Lau, N. C., 1981. A diagnostic study of recurrent meteorological anomalies appearing in a 15-year simulation with a GFDL general circulation model, *Mon. Wea. Rev.* 109, 2287–2311.

Lau, N. C., 1985. Modeling the seasonal dependence of the atmospheric response to observed El-Niños in 1962–76, *Mon. Wea. Rev.* 113, 1970–1996.

Lau, N. C. and Oort, A. H., 1984. Response of a GFDL general circulation model to SST fluctuations observed in the tropical Pacific Ocean during the period 1962–1976, in *Coupled Atmosphere–Ocean Models*, Elsevier, New York.

Malone, R. C., Pitcher, E. J., Blackmon, M. L., Puri, K., and Bourke, W., 1984. The simulation of stationary and transient geopotential height eddies in January and July with a spectral general circulation model, *J. Atmos. Sci.* 41, 1394–1419.

Manabe, S. and Hahn, D. G., 1981. Simulation of atmospheric variability, *Mon. Wea. Rev.* **109**, 2260–2286.

Manabe, S. and Smagorinsky, J., 1967. Simulated climatology of a general circulation model with a hydrologic cycle. II. Analysis of the tropical atmosphere, *Mon. Wea. Rev.* **95**, 155–169.

Manabe, S., Hahn, D. G., and Holloway, J. L., 1974. The seasonal variation of the tropical circulation as simulated by a global model of the atmosphere, *J. Atmos. Sci.* **31**, 43–83.

Manabe, S., Hahn, D. G., and Holloway, J. L., 1979. Climate simulations with GFDL spectral models of the atmosphere: Effect of spectral truncation, in *GARP Publication Series No. 22*, World Meteorological Organization, Geneva, Switzerland.

Manabe, S., Holloway, J. L., and Stone, H. M., 1970. Tropical circulation in a time-integration of a global model of the atmosphere, *J. Atmos. Sci.* **27**, 580–613.

Mansfield, D. A., 1981. The incidence of blocking in the Meteorological Office's 5-level model, *Met. 0.13 Branch Memorandum No. 99*, Meteorological Office, Bracknell, England.

Mintz, Y., 1984. The sensitivity of numerically simulated climates to land-surface boundary conditions, in John T. Houghton, Ed. *The Global Climate*, Cambridge University Press, London.

Mintz, Y. and Dean, G., 1952. The observed mean field of motion of the atmosphere, *Geophys. Res. Papers* **17**, 1–65.

Moura, A. and Shukla, J. 1981, On the dynamics of droughts in northeast Brazil, observation, theory, and numerical experiments with a general circulation model, *J. Atmos. Sci.*, **38**, 2653–2675.

Philander, S. G. H. and Seigel, A., 1985. Simulation of the El Niño of 1982–1983, Proceedings of the 16th International Liège Colloquium on Hydrodynamics, in *Coupled Atmosphere–Ocean Models*, Elsevier, New York.

Pitcher, E. J., Malone, R. C., Ramanathan, V., Blackmon, M. L., Puri, K., and Bourke, W., 1983. January and July simulations with a spectral general circulation model, *J. Atmos. Sci.* **40**, 580–604.

Sadler, J. C., 1975. *The Upper Tropospheric Circulation over the Global Tropics*, Department of Meteorology, University of Hawaii, Report No. UHMET 75-05, pp. 1–35.

Shukla, J., 1981a. Dynamical predictability of monthly means, *J. Atmos. Sci.* **38**, 2547–2572.

Shukla, J., 1981b. Predictability of the tropical atmosphere, *NASA Technical Memo. No. 83829*, Goddard Space Flight Center, Greenbelt, MD, pp. 1–51.

Shukla, J. and Mo, K. C., 1983. Seasonal and geographical variation of blocking, *Mon. Wea. Rev.* **111**, 388–402.

Shukla, J. and Mintz, Y., 1982. Influence of land-surface evapotranspiration on the earth's climate, *Science* **215**, 1498–1501.

Shukla, J. and Wallace, J. M., 1983. Numerical simulation of the atmospheric response to equatorial Pacific sea surface temperature anomalies, *J. Atmos. Sci.* **40**, 1613–1630.

Shukla, J., Straus, D., Randall, D., Sud, Y., and Marx, L., 1981a. Winter and summer simulations with the GLAS climate model, *NASA Technical Memo. 83866* (NTIS N821880), Goddard Space Flight Center, Greenbelt, MD.

Shukla, J., Mo, K. C., and Eaton, M., 1981b. Climatology of blocking in the GLAS climate model, *NASA Technical Memo. No. 83907*, Goddard Space Flight Center, Greenbelt, MD, pp. 207–216.

Tung, K. K. and Lindzen, R. S., 1979. A theory of stationary longwaves. Part I. A simple theory of blocking, *Mon. Wea. Rev.* **107**, 714–734.

☐ COMMENTS ON "GENERAL CIRCULATION MODELING AND THE TROPICS"

James E. Hansen

Shukla has done a good job of describing numerical results obtained with a typical general circulation model. I therefore confine my comments to (1) several remarks about GCM studies that have been used to analyze physical processes in the tropics and (2) some questions concerning the reliability of GCM simulations of climate change in the tropics.

Early GCM studies were focused mainly on middle latitudes, but useful insight regarding tropical circulation has been provided in the past decade by certain GCM experiments. These experiments illustrate that a good deal can be learned from GCM experiments provided that the user focuses on general conclusions that are independent of model details and imperfections.

Charney et al. (1975) examined the effect of a regional-scale increase in surface albedo, such as may occur with defoliation or deforestation of vegetated land. They found that the increase of surface albedo leads to increased radiative cooling by the atmosphere, increased local subsidence, and thus a suppression of cumulus convection and its associated rainfall. Since reduced rainfall would tend to further reduce vegetation cover, the process represents a positive-feedback mechanism. The process is most likely to be important in arid or semiarid regions where large-scale subsidence already occurs, where most of the rainfall is from cumulus clouds, and where transports by the winds are weak and inefficient at counteracting temperature changes due to the albedo change. Reduced vegetation cover also reduces the potential for local evapotranspiration, and this too tends to contribute to the positive feedback. Therefore, at least in areas of marginal precipitation, there appears to be a real possibility that anthropogenic desertification may tend to feed on itself, creating a chronic problem of inadequate rainfall. Although the natural variability of rainfall in the tropics is so large that wet years and dry years will always occur, the GCM experiments suggest that it is important to better understand the relation between anthropogenic effects on vegetation cover and regional climate. Obtaining such understanding will require more realistic modeling of the biosphere in GCMs than that done to date.

GCM experiments have also revealed information on the mechanisms that drive the large-scale longitudinal (Walker) and meridional (Hadley) circulation in the tropics. Manabe and Terpstra (1974) did an experiment in which they removed all mountains on the globe. They found that the mountains cause a great deal of long-wave stationary eddy energy in the atmosphere but have little effect on the total eddy energy, which is dominated by smaller-scale transient eddy energy in the no-mountain case. Topography was also found to cause cyclogenesis on the lee side of major mountain ranges and to affect the global distribution of precipitation by altering the three-dimensional advection of moisture. However, the large changes were all at middle and high latitudes; the tropical circulation and hydrological cycle were found to be much less dependent on topography.

A series of GCM experiments were made by Stone and Chervin (1984) and Chervin and Druyan (1984) in which they investigated systematically the roles of continentality, sea surface temperature gradients, and topography in maintaining the tropical Walker circulation. They found that the primary factor affecting the Walker circulation in the model is the global distribution of continents and oceans; ocean surface temperature gradients were found to also be important, but topography was relatively unimportant, the latter conclusion being consistent with the experiment of Manabe and Terpstra (1974). The Stone and Chervin (1984) experiments show that both continentality and ocean surface temperature gradients force the model atmosphere by modifying the surface heat balance. Where the atmosphere is heated, rising motions are generated, causing convergence of moisture and condensation, the resulting heating of the atmosphere reinforcing the rising motion. The vertical motions were found to be highly correlated with the surface heating and precipitation, and the precipitation was correlated more with moisture convergence than with evaporation. One very interesting conclusion from these experiments was that the forcing by ocean surface temperature gradients contains a large nonlocal component; that is, the changes in the local heat balance and forcing of the atmosphere can, to a large extent, depend on nonlocal changes in ocean surface temperatures. Indeed, in the south tropical Pacific, the model response was greatly enhanced by the continentality and was controlled more by distant ocean surface temperature gradients than by local ocean surface temperature gradients.

A series of experiments was made by Rind and Rossow (1984) to investigate the effects of different physical processes on the Hadley circulation. These experiments included changes such as "turning the sun off," eliminating sea surface temperature gradients, eliminating evaporation, eliminating surface friction, and eliminating mixing of momentum by convection. The results indicate that the Hadley circulation responds to both thermal and momentum forcing, but the response tends to be complicated, with adjustments among the several processes that force the Hadley circulation taking place in response to changes of a single process. The occurrence of these adjustments suggests that prediction of the effects of anthropogenic

surface perturbations on the Hadley circulation will depend on the availability of models with realistic representation of complex atmospheric processes and their interactions.

The above studies are examples of cases in which useful insights about tropical circulation and climate have been derived from GCM studies. But are GCMs capable of reliable simulation of the effects of changes, anthropogenic or otherwise, of vegetation or other surface conditions? It will be relatively easy to incorporate into the GCMs representations of the biosphere and surface that are as detailed as the biologists care to contribute. This will undoubtedly permit some interesting sensitivity studies and general conclusions of the type obtained in the studies discussed above. However, it should not be assumed that GCMs will be ready for reliable assessment of the climatic impact of regional surface perturbations. Quite apart from the possibility that such assessments may require much higher spatial resolution than that employed in current GCMs, there are serious questions about how well present models represent first-order atmospheric processes.

One area of particular concern is the parameterization of moist convection for GCMs. Baker et al. (1978) tried two different parameterizations of moist convection, a convective adjustment scheme and a more elaborate convective parameterization of Kuo (1974), finding a strong sensitivity to the convective parameterization in 10-day forecasts, probably resulting from differences in the release of latent heat. We also note that forecasts made with the model of the European Centre for Medium Range Weather Forecasts (ECMWF), which has been shown to be more accurate than other current operational forecast models, are very much less accurate in the tropics than at higher latitudes (Bengtsson and Simmons, 1983). Assessments of the model forecasts by the ECMWF group lead them to suggest that there are serious deficiencies in their parameterizations of convection. Bengtsson and Simmons (1983) conclude that tropical forecasts respond more quickly and acutely to defects in the model than do forecasts at middle and high latitudes.

The need for a better understanding of the GCMs in tropical regions and for improvements in the representations of physical processes apparently is not limited to short-range forecasts. The GCM experiments with doubled CO_2 by Manabe and Stouffer (1980) and Hansen et al. (1984) yield relatively similar climate sensitivities at high latitudes but differences of more than a factor of 2 at low latitudes. Differences in clouds and convection in the models are a likely explanation for the difference in sensitivity, but whether either model has a realistic tropical climate sensitivity is open to question.

In this short comment, it is not practical to discuss satisfactorily how well current GCMs simulate tropical climate, and I have omitted major topics such as modeling of the El Niño, which, however, is included in Shukla's review. I only note that although GCMs have been used to infer valuable information on certain weather and climate processes in the tropics, there is still a great need for improvement in our understanding of current models and for improvement of the models. It is not at all clear that the modeling

tools are yet in hand for reliable assessment of the interactions between man, the biosphere, and climate in the tropics.

ACKNOWLEDGMENTS

I am particularly indebted to my colleagues Drs. Peter Stone and David Rind for their suggestions and comments.

REFERENCES

Baker, W. E., Kung, E. C., and Somerville, R. C. J., 1978. An energetics analysis of forecast experiments with the NCAR general circulation model, *Mon. Wea. Rev.* **106**, 311–323.

Bengtsson, L. and Simmons, A. J., 1983. Medium-range weather prediction—operational experience at ECMWF, in B. Hoskins and R. Pearce, Eds., *Large-Scale Dynamical Processes in the Atmosphere*, Academic, New York.

Charney, J., Stone, P. H., and Quirk, W. J., 1975. Drought in the Sahara: A biogeophysical feedback mechanism, *Science* **187**, 434–435.

Chervin, R. M. and Druyan, L. M., 1984. The influence of ocean surface temperature gradient and continentality on the Walker circulation. Part I: Prescribed tropical changes, *Mon. Wea. Rev.* **112**, 1510–1523.

Hansen, J., Lacis, A., Rind, D., Russell, G., Stone, P., Fung, I., Ruedy, R., and Lerner, J., 1984. Climate sensitivity: Analysis of feedback mechanisms, in J. Hansen and T. Takahashi, Eds., *Climate Processes and Climate Sensitivity*, American Geophysical Union, Washington, DC.

Kuo, H. L., 1974. Further studies of the parameterization of the influence of cumulus convection in large-scale flow, *J. Atmos. Sci.* **31**, 1232–1240.

Manabe, S. and Stouffer, R. J., 1980. Sensitivity of a global climate model to an increase of CO_2 concentration in the atmosphere, *J. Geophys. Res.* **85**, 5529–5554.

Manabe, S. and Terpstra, T. B., 1974. The effects of mountains on the general circulation of the atmosphere as identified by numerical experiments. *J. Atmos. Sci.* **31**, 3–42.

Rind, D. and Rossow, W. B., 1984. The effects of physical processes on the Hadley circulation, *J. Atmos. Sci.* **41**, 479–507.

Stone, P. H. and Chervin, R. M., 1984. The influence of ocean surface temperature gradient and continentality on the Walker circulation. Part II: Prescribed global changes, *Mon. Wea. Rev.* **112**, 1524–1534.